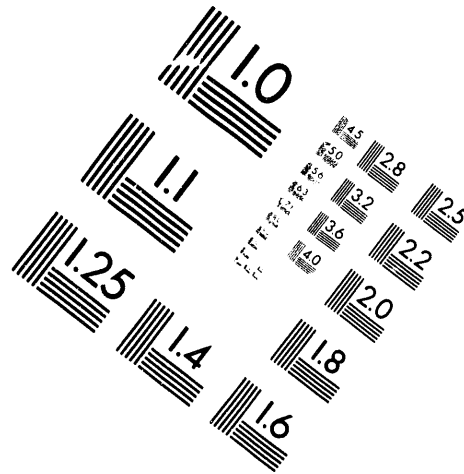
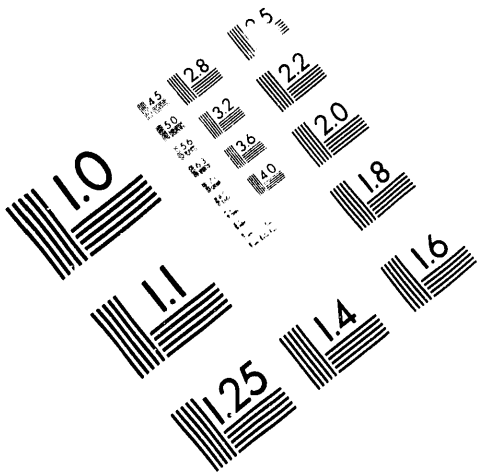




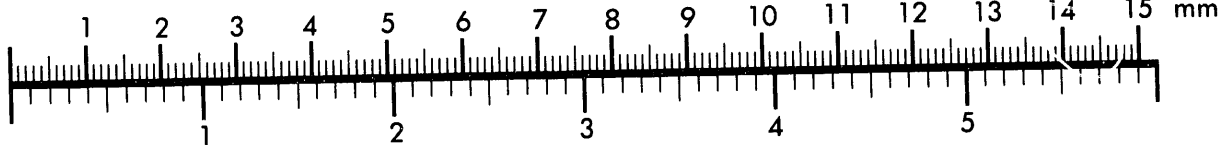
AIM

Association for Information and Image Management

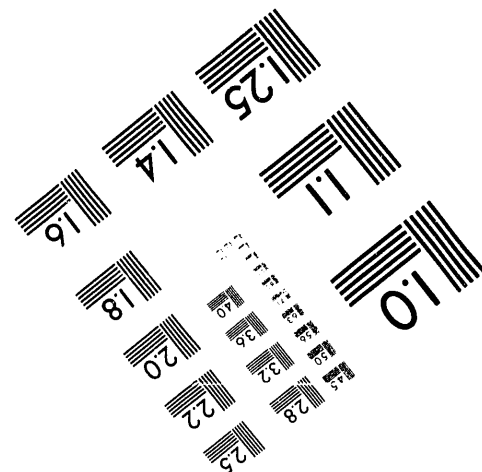
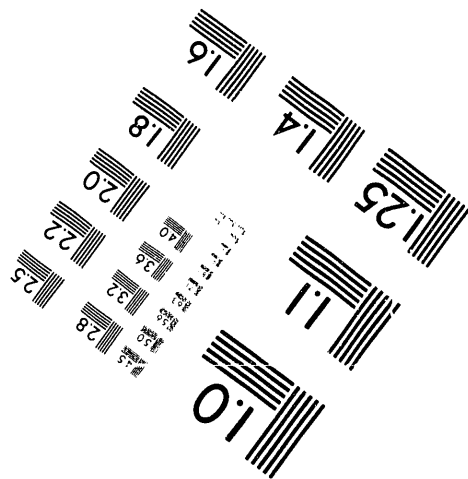
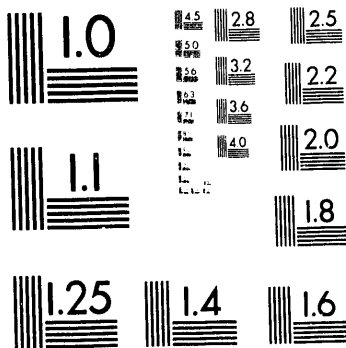
1100 Wayne Avenue, Suite 1100
Silver Spring, Maryland 20910
301/587-8202



Centimeter



Inches



MANUFACTURED TO AIM STANDARDS
BY APPLIED IMAGE, INC.

1 of 1

49/8-93 JSD

PREPARED FOR THE U.S. DEPARTMENT OF ENERGY,
UNDER CONTRACT DE-AC02-76-CHO-3073

PPPL-2903
UC-420.423

PPPL-2903

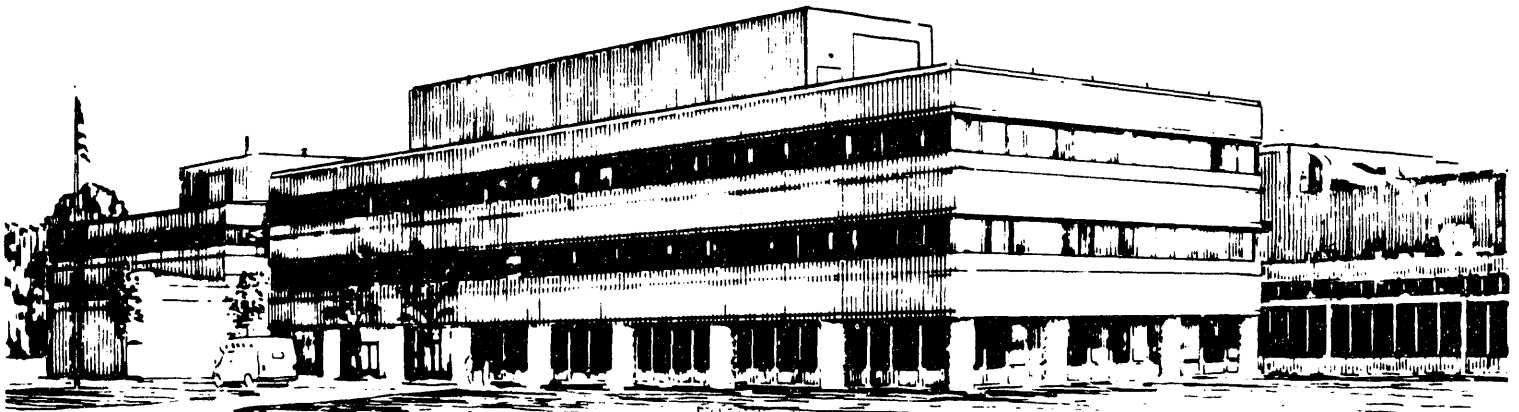
INITIAL BORONIZATION OF PBX-M USING ABLATION
OF SOLID BORONIZED PROBES

BY

H.W. KUGEL, Y. HIROOKA, J. TIMBERLAKE, ET AL.

MAY, 1993

PPPL PRINCETON
PLASMA PHYSICS
LABORATORY



DISSEMINATION OF THIS DOCUMENT IS UNLIMITED

PRINCETON UNIVERSITY PRINCETON NEW JERSEY

NOTICE

This report was prepared as an account of work sponsored by an agency of the United States Government. Neither the United States Government nor any agency thereof, nor any of their employees, makes any warranty, express or implied, or assumes any legal liability or responsibility for the accuracy, completeness, or usefulness of any information, apparatus, product, or process disclosed, or represents that its use would not infringe privately owned rights. Reference herein to any specific commercial produce, process, or service by trade name, trademark, manufacturer, or otherwise, does not necessarily constitute or imply its endorsement, recommendation, or favoring by the United States Government or any agency thereof. The views and opinions of authors expressed herein do not necessarily state or reflect those of the United States Government or any agency thereof.

NOTICE

This report has been reproduced from the best available copy.
Available in paper copy and microfiche.

Number of pages in this report: 41

DOE and DOE contractors can obtain copies of this report from:

Office of Scientific and Technical Information
P.O. Box 62
Oak Ridge, TN 37831;
(615) 576-8401.

This report is publicly available from the:

National Technical Information Service
Department of Commerce
5285 Port Royal Road
Springfield, Virginia 22161
(703) 487-4650

Initial Boronization of PBX-M Using Ablation of Solid Boronized Probes

H. W. Kugel, Y. Hirooka,¹⁾ J. Timberlake, R. Bell, A. England,²⁾
R. Isler,²⁾ S. Jones,³⁾ R. Kaita, S. Kaye, M. Khandagle,¹⁾
M. Okabayashi, S. Paul, H. Takahashi, W. Tighe,
S. von Goeler, and A. Post-Zwicker²⁾

Princeton Plasma Physics Laboratory,
Princeton University, Princeton, NJ 08543

1) IPFR, University of California at Los Angeles, Los Angeles, CA 90024

2) Oak Ridge National Laboratory, Oak Ridge, TN 37831

3) Massachusetts Institute of Technology, Cambridge, MA 02139

Abstract

The initial boronization of PBX-M was performed using the sequential ablation of two types of solid target probes. Probe-1 in a mushroom shape consisted of a 10.7% boronized 2-D C-C composite containing 3.6 g of boron in a B₄C binder. Probe-2 in a rectangular shape consisted of an 86% boronized graphite felt composite containing 19.5 g of 40 μ boron particles. After boronization with Probe-1, the loop voltage during 1 MW neutral beam heated plasmas decreased 27% and volt-sec consumption decreased 20%. Strong peripheral spectral lines from low-Z elements decreased by factors of about 5. The central oxygen density decreased 15-20%. The total radiated power during neutral beam injection decreased by 43%. Probe-2 boronization exhibited improved operating conditions similar to Probe-1, but for some parameters, a smaller percentage change occurred due to the residual boron from the previous boronization using Probe-1. The ablation rates of both probes were consistent with front face temperatures at or slightly above the boron melting point. These results confirm the effectiveness of the solid target boronization (STB) technique as a real-time impurity control method for replenishing boron depositions without the use of hazardous borane compounds.

1. Introduction

The long-term objective of the Princeton Beta Experiment-Modified (PBX-M) is the development of an advanced tokamak configuration able to access the full volume, high-beta, 2nd stability regime of tokamak confinement.[1,2] Improving PBX-M impurity control and edge plasma parameters are important for enhancing access to the 2nd stability regime over the full plasma volume. The deposition of thin boron films ("boronization") has been shown to be an effective method for controlling oxygen, carbon, metal, and other deleterious impurities in tokamaks.[3-8] Typical boronization methods apply plasma assisted chemical vapor deposition (PCVD) of boron from hazardous borane compounds.[3-8] These methods involve several difficult technical, environmental, safety, and health issues.[9]

In PBX-M, for example, there are technical constraints on the application of previous boronization techniques which include an unbakeable vessel and a complex interior that includes a closely-fitting electrically isolated passive plate system, RF antennas, coils, cabling, and instrumentation. In addition, recent environmental, safety, and health (ES&H) regulatory requirements further limit the available options for PBX-M which has a relatively open test cell. Recently, many of these operational difficulties were avoided by the application of the solid target boronization (STB) technique on the Tokamak de Varennes (TdeV).[10] A solid target probe of boronized carbon-carbon (C-C) composite was inserted in the edge plasma region to produce decomposition/evaporation of boron carbide. This boron deposition resulted in a significant improvement in plasma performance.[10] Following the TdeV work, STB experiments with low ablation rates were performed on the MST reversed-field pinch using a sintered B_4C rod target.[11] In the present work, we report the results of the initial boronization of PBX-M using the sequential ablation of two types of STB probes.

2. Experiment

2.1. Probe-1 Configuration

The selection of a material for an STB probe from the available candidate materials having a wide range in boron content involves several technical issues. Boronized C-C composites and boronized graphite composites, for example, can be prepared by the heat processing of a woven C-C material or graphite base with suitable boron compounds and binders. Selecting a composite with a low boron-to-

carbon ratio allows for convenient machining and fabrication. The use of a low boron-to-carbon ratio, however, requires sufficient heating to overcome heat losses through the matrix, but this may be easily obtainable in high temperature edge plasma conditions. Increasing the boron-to-carbon ratio beyond about 40% makes the resulting material hardness difficult to machine or render by conventional methods. The use of boron ceramic materials with very high boron-to-carbon ratios is promising but introduces additional difficulties. This is usually material with a poor thermal conductivity which requires cautious slow heating and cooling so as not to cause fracturing from cyclic thermal stress, and consequently, may not yield high boron deposition rates.[11]

In this work, the first probe (Probe-1) applied to the initial boronization of PBX-M consisted of a mushroom shaped carbon-carbon (C-C) composite containing 10.7% atomic boron in the form of B_4C in the binder material with a total of about 3.6 g of boron. A similar probe, consisting of a C-C composite containing 30% boron obtained from the same commercial source was used on the TdeV.[10] Figures 1(a) and 1(b) are photographs showing side and front views, respectively, of Probe-1 after exposure. Shown is the boronized C-C composite mounted on an isotropic graphite base. Figure 2 shows the results of energy-dispersive type characteristic x-ray analysis of the boron atomic percentages at the indicated surface positions before and after exposure. It is seen that after exposure, the boron is totally depleted in the central region. The boron depletion region appears to be inclined towards the direction of the incident ion current, and there is an indication of redeposition of boron on the opposite side. An analysis of the microstructures of erosion and redeposition surfaces will be published separately.[12] The discloration of the boron depleted region can be seen in Figure 1(b) at the center of the probe tip. Inspection of this region under magnification showed clearly the weave of the C-C composite and some inter-weave spaces depleted of binder material down to depths of about 1 to 2 mm.

The probe unit assembly was held by an electrically floating vacuum feed-through mechanism and inserted into PBX-M via a bellows mechanism. The electrical isolation was provided to prevent possible deleterious current flows during a plasma disruption. After passage through the torus interface valve, Probe-1 was positioned inside the vessel, at the outer wall (major radius $R = 207$ cm), for several hours. This procedure allowed the probe to be heated slowly and to undergo any residual outgassing before insertion beyond the last closed flux surface (LCFS) at about $R=194.8$ cm. Bean-shaped, indented, 250 kA, neutral beam-heated plasmas were established. The discharge repetition time was 240 sec. The probe was then slowly

inserted into the edge plasma over a total of about 40 plasma discharges (shots) each lasting about 0.75 sec, to an eventual depth of about 192.2 cm, or about 2.6 cm beyond the LCFS. In the case of STB experiments on TdeV, the target was inserted to a position about 2 cm inside the LCFS.[10] During the insertion of Probe-1, the incandescence of the probe was viewed and recorded using a plasma TV camera. In addition, bremsstrahlung x-rays emitted from outwardly diffusing fast electrons incident on Probe-1 during very low power ($\sim \leq 100$ kW) Lower Hybrid Current Drive (LHCD) testing during the boronization were observed with a 2-Dimensional Hard X-ray Imaging system.[13]

2.2. Probe-1 Results

Figure 3 shows the Probe-1 major radius position (cm) and the relative intensities of the B III and O II impurities from 600 to 620 msec versus shot number. The spectral measurements were made at a location 180° toroidally from the probe position. At this position, the spectrometer could not view the probe due to the center column of the machine. Hence, the measured boron intensities can be attributed to boron transport in the outer region of the plasma. At shot No. 295714, 300 msec neutral beam injection started at a relatively low power level (0.32 MW) and reached 1 MW, 8 shots later. It is seen in Figure 3 that as Probe-1 was slowly inserted into the plasma, beyond the LCFS ($R < 194.8$ cm), the B III intensity started increasing and the O II intensity started decreasing. A similar shot-to-shot behavior was observed in TdeV.[10] This is believed to be the process in which surfaces are slowly covered with boron, thereby enhancing the gettering effect of oxygen. The B III emission rose and reached a maximum plateau. The O II intensity reached a minimum plateau. Later, as Probe-1 reached maximum insertion (at $R = 192.2$ cm) and the neutral beam injected power was still at 1 MW, the O II emission continued dropping and eventually decreased by a factor of about 4.5. After about shot No. 295750, with the probe at its maximum depth, the B III intensity started falling, and the O II intensity rose to about half of its original value within a few shots. This decrease in B III intensity is attributed to boron depletion in the probe tip, as discussed below. This indicates that the depletion rate observed in PBX-M was more rapid than that observed in TdeV, i.e., 10.7% boron depleted in 40 shots in PBX-M and 30% boron depleted in 240 shots in TdeV [10]. The rise in the O II intensity may have been due to the decrease in the boron yield and additional impurities generated by several plasma current disruptions between the O II intensity minimum and its final rise. Figure 4 shows spectral intensities in the visible region for

Probe-1 during neutral beam injection from 600 to 620 msec, (a) before and (b) during boronization, respectively. It is seen that significant boron emission occurred at a toroidal point 180° from the probe. Figure 5 shows the time evolution of O II and B III intensities for the same shots (a) before and (b) during boronization, respectively. During boronization, the B III intensity increased significantly during neutral beam injection (400 ms to 700 ms), as the edge plasma heated and enhanced the evaporation of boron.

Figure 6(a) shows spectral intensities in the UV region for Probe-1 during neutral beam injection before boronization and Figure 6(b) during boronization. The UV emission of oxygen and fluorine intensities followed the same behavior with shot number as the O II intensity in the visible region. The origin of the fluorine contribution was from the accidental exposure of teflon insulation in the vessel. An increase in the edge Fe intensity was observed during boronization (Figure 6(b)). Similar metal radiation increases were observed in the W-AS-VII stellarator after the first boronization and attributed to the hotter edge conditions.[14] Figures 7 and 8 show the decrease in selected UV region spectral intensities with shot number. The fluorine F VI and F VII intensities (referred to above), decreased by a factor of about 5, and the oxygen O V and O VI intensities decreased by a factor of 5 to 6. Measurements of the radial profiles of O VIII intensities from charge-exchange excitation (CXE) indicated that after boronization, the O VIII densities at the edge decreased by a factor of 2. The change in central O VIII densities during these conditions was small, 15-20%, and is still under investigation.

Figure 9(a) shows the 20% reduction in single turn loop voltage that occurred after boronization for a 240 kA ohmically heated fiducial plasma. The corresponding decrease in volt-second consumption was 10%. Figure 9(b) shows the 29% reduction in single turn loop voltage that occurred after boronization for a 250 kA, 1.1 MW neutral beam heated plasma. The corresponding decrease in volt-second consumption for this case was 20%. Tangential bolometer measurements indicate that after boronization the total radiated power during neutral beam injection decreased 43%.

Z-effective and electron temperature measurements have not been performed yet. The central ion temperature measured from CXE of O VIII increased by a factor of about 1.3.

Similar percentage decreases in oxygen radiation and improvements in important operating parameters were observed in TdeV after boronization using the STB technique [10], and in other tokamaks with different internal geometries, operating procedures, and vacuum wall conditions after boronization using the PCVD technique [3-8].

2.3 Probe-2 Configuration

Two days after the Probe-1 boronization, the second probe (Probe-2), in a rectangular shape and employing a different embodiment of the STB technique was applied to PBX-M. This composite graphite probe was developed for fast deposition of thin films of boron and other materials during conditions of high thermal shock. In particular, for effective boron evaporation, the selected probe material was a thickly-woven, high-purity graphite felt having a thermal conductivity a factor of 2000 lower than that of conventional graphite and a high resistance to thermal shock. These thermal insulating and shock resistant properties were useful for retaining applied heat and allowing the target material to be heated rapidly by a few ohmic discharges to temperatures yielding high ablation rates. The ability to retain heat and maintain high temperature between discharges also provided the option of gradually achieving high temperatures with minimal penetrations into the scrape-off layer. The graphite felt used in the fabrication of Probe-2 possessed a weave that was sufficiently thick, and yet was sufficiently porous within the weave, to hold large quantities of the impregnated boron. The graphite felt was cut to the desired rectangular shape of 2.5 cm x 5.0 cm by 1.3 cm thick. Two such pieces (1.3 cm thick) were placed together in a special graphite holder so as to form one rectangular piece with the dimensions 2.5 cm x 5.0 cm by 2.5 cm thick. Figure 10(a) shows a top side view of Probe-2 held in its C-C composite holder after exposure to PBX-M plasmas and the boronization discussed below. Shown is the melted boron at the tip of the graphite felt. The small separation near the front face at the center of the graphite felt is between the two 1.3 cm thick pieces used to fabricate the probe as described below. This separation may have occurred as a result of the melting effect of the boron. Figure 10(b) shows Probe-2 with a view on the side facing the incident ions. Shown is the melted boron and the increased ablation on the side facing the incident ion direction. Measurements before and after exposure indicated that the overall length of the graphite felt probe was about the same, and that the net weight loss due to exposure was 1 g. Since the length of the probe remained about the same, and since as discussed below in Section 3, the boron has significantly higher evaporation rates at a given temperature than graphite, this weight loss was attributed predominantly to the ablation 1 g of boron or 5.6×10^{22} atoms from the initial loading of 19.5 g of boron.

The boron introduced into the graphite consisted of 40 μ boron powder. The powder was mixed with ethyl alcohol in a beaker forming a suspended colloid-like

mixture. The tip of the graphite felt electrode was then immersed in the liquid mixture, which was readily absorbed by the graphite felt, in a wick-like manner. The wet electrode was then air dried in an oven for 1 hour at 100-120 °C, thereby evaporating the alcohol and fixing the boron powder within the porous maze of the graphite felt. The process was then repeated three times. Each time the liquid ethyl alcohol was able to transport additional boron into the porous maze of the graphite felt until eventually saturation appeared imminent. Saturation was evidenced by the eventual appearance of loose boron powder on the surface of the electrode. Tests showed that the graphite felt probe could achieve a boron holding capacity of about 86% boron by weight before reaching saturation. The total amount of boron loaded was 19.5 g. The graphite felt with this boron loading exhibited to the eye no evidence of its boron contents. Other tests, providing a mechanical impact to a similar boron loaded probe, demonstrated the ability of the graphite felt matrix to hold its boron contents beyond the demands of a tokamak environment. The boron-loaded graphite felt electrode, prepared in the above manner, was then inserted into a vacuum chamber for outgassing. Typically, vacuum pressures in the low 10^{-7} Torr range were achieved after pumping for 24 hours or less, indicating that the probe was relatively free of volatile components.

The insertion of Probe-2 followed an outgassing procedure similar to that described above for Probe-1. Bean-shaped, indented 240 kA ohmic plasmas were established. Probe-2 was slowly inserted into the edge plasma, in steps of about 0.1 to 0.2 cm, for a total of about 26 PBX-M plasma pulses to an eventual depth of 192.5 cm, or about 2.3 cm beyond the LCFS. During this operation, as in the case of Probe-1, the incandescence of the probe was viewed and recorded using a plasma TV camera, and bremsstrahlung x-rays emitted from outwardly diffusing fast electrons incident on Probe-2 during low power (~100-300 kW) LHCD testing during the boronization were observed.[13]

2.4. Probe-2 Results

Figure 11 shows the Probe-2 major radius position (cm) and the relative intensities of the B III and O II components versus shot number. As noted above for the case of Probe-1, the spectral measurements were made at a location 180° from the probe position. Hence, the measured boron intensities can be attributed to boron transport in the outer region of the plasma. As Probe-2 was slowly inserted beyond the LCFS at about 194.8 cm during ohmic heating, the B III intensity rose rapidly. The O II intensity (multiplied by x3 for convenient display) decreased directly as the B III

intensity increased. The B III intensity started to decrease after shot No. 296235 due to short disruptive plasma discharges, and the O II intensity started to increase. At about shot No. 296241, the second large increase in B III started as 0.8 MW of neutral beam injection was introduced. The injection power reached 1.8 MW on the next shot, and increased to 2 MW by shot No. 295249. O II intensities also started increasing after shot No. 296240, as the probe was moved outward, and as wall outgassing due to injected neutral beam power increased between shots No. 296241 and No. 296245. Then H-modes started to occur at shot No. 296247, and the O II intensity started a fast rise to a peak value of about half of its original value. These H-modes started as Probe-2 was moved outward after shot No. 296245, and the B III intensity started decreasing as boron ablation from the probe decreased. The incandescent glow of Probe-2, which lasted over 4 seconds after the plasma current pulse, was observed with the visible TV camera. As the probe was withdrawn (after shot No. 296250), the incandescence decreased and no glow was observed after shot No. 296254. In addition, no B III intensity was observed during normal discharges after shot No. 296254, and the final O II intensity was 1/3 to 1/2 of the original value. Although the B III intensity was not observed during normal discharges after shot No. 296254, the B III signal continued to be observed during disruptions for many subsequent discharges. This suggests that power liberated during disruptions was reaching boron not accessible to normal plasma surface interactions.

The Probe-2 visible spectroscopic results were very similar to those obtained for Probe-1. Figure 12(a) shows the visible spectral intensities during ohmic discharges before boronization, and Figure 12(b) during boronization. As in the case of Probe-1, these signals indicated that significant boron emission was observed at a toroidal point 180° from the probe. Figure 13 shows the time evolution of O II and B III intensities for the same ohmically heated discharges (a) before and (b) during boronization, respectively. Before boronization, the O II intensity increased during the discharge. During boronization, the O II intensity was relatively low due to the preceding boron depositions and the additional evaporation of boron.

The Probe-2 UV spectroscopic results were very similar to those obtained for Probe-1. Figure 14(a) shows the spectral intensities for Probe-2 in the UV region during ohmically heated discharges before boronization and Figure 14(b) during boronization. In general, in the UV spectral region, the carbon, oxygen, and fluorine intensities followed the same behavior with shot number as the O II intensity in the visible spectrum. As during Probe-1 boronization, an increase in edge Fe emission

was observed during Probe-2 boronization (Figure 14(b)) due to hotter edge conditions.[14]

2.5 Results after Boronization with Probe-1 and Probe-2

PBX-M employs titanium gettering in the lower dome of the vacuum vessel. This gettering is initiated at the beginning of each operating day and continues between discharges. After several hours of titanium gettering, the PBX-M vacuum base pressure was reduced typically by about a factor of 10 to 20 to the low 10^{-8} Torr range. The morning after the final boronization, the vacuum base pressure in the PBX-M vessel was comparable to that achieved only after several hours of titanium gettering. This is attributed to the wall pumping of impurities due to the deposited boron. Over the following non-operating day, an air leak occurred which vented the vessel to the low 10^{-6} Torr range. After correcting this vacuum leak, normal plasma operations resumed. Using these wall conditions, post boronization measurements of neutron production rates were made during neutral beam heated plasmas for IBW experiments then in progress. Figure 15 shows the average D-D neutron production rates measured during these experiments for 300 msec neutral beam heated discharges during 10 weeks of operation before boronization, during Probe-1 boronization, and during the third operating day after Probe-1 plus Probe-2 boronizations. Proceeding from left to right in Figure 15, the first 10 measurements during Probe-1 boronization (open squares) occurred in temporal sequence as the neutral beam injection power was raised for each successive discharge from 0.4 MW to 1 MW. Toward the end of the final discharges at 1 MW, lower yields were measured as boron was depleted from Probe-1 during the final 12 shots (discussed above). A similar effect occurred after boronization with Probe-1 and Probe-2 (open circles). The highest neutron rates measured at 2 MW were for the initial neutral beam heated discharges, but the subsequent neutron rates, under relatively constant plasma conditions over about 60 shots, decreased slowly as boron was eroded from plasma surfaces. The possible effect of other changes is still under investigation. Although the overall results shown in Figure 15 include different experimental conditions during a 12 week operating period, the neutron production rates measured during Probe-1 boronization, and after the final boronization tended to be comparable to the highest values obtained prior to boronization. Although the various factors influencing the measured variations in neutron production rates are still under investigation, these preliminary results suggest that if boronization is combined with more optimum neutron production conditions, higher neutron yields might be obtained.

3. Discussion

A weight loss measurement is not available for Probe-1. The Probe-2 weight loss was used to calibrate the boron ablation rate and to infer the net boron deposition amounts for both probes. Figure 16 shows boron evaporation rates (atoms/cm²-sec) from pure boron and B₄C versus temperature (°K) derived from previously measured vapor pressures using the Knudsen equation.[16-20] The present results and previous measurements imply that a negligible amount of the graphite felt matrix was ablated relative to the amount of ablated boron. At the boron melting point of 2573 °K, the graphite evaporation rate is a factor of 10⁻⁴ lower than that of pure boron.[21] Radiation enhanced sublimation (RES) could increase the graphite sublimation rates but little is known about these effects at temperatures near and above the melting point of boron.[15] Probe-2, after exposure, exhibited a region of solid, crystalline-like boron at the front face of the probe resembling a melted boron flow toward the front face, followed by solidification after intense melting (Figures 10(a) and 10(b)). Also, measurements indicated that the overall length of the graphite felt was about the same before and after exposure. Spectroscopic measurements as Probe-2 was inserted found that carbon levels increased for 3 or 4 discharges but then appeared to follow the decrease in oxygen. These results suggest that the measured Probe-2 weight loss of 1 g can be attributed primarily to the loss of boron and a negligible amount of the graphite felt matrix.

The Probe-2 weight loss of 1 g occurred initially over about 14 ohmic pulses of 750 msec duration, followed by 12 NBI pulses of duration 300 msec (Figure 11). During the NBI pulses, Probe-2 was withdrawn to a larger major radius and the resulting B III intensity measured on the opposite side of the torus, at 600 msec into the discharge was comparable but smaller than that measured during the ohmic pulses (Figure 11). The total integrated B III intensity during the longer ohmic pulses was 2.7 greater than emitted during the shorter, neutral beam pulses with the probe farther out. Assuming to first order, a proportionality between these total B III emissions and the ablated boron mass implies 730 mg of boron ablated during the ohmic pulses and 270 mg ablated during the NBI pulses. The boron melting exhibited in Figure 10(b) occurred over about 10 cm² of the front face and front sides of Probe-2. Therefore, during the ohmic pulses the boron evaporation rate was about 8 x 10⁻³ g/cm²-sec, or 4.5 x 10²⁰ atoms/cm²-sec. During the NBI discharges, the boron evaporation rate was about 6.5 x 10⁻³ g/cm²-sec, or 3.6 x 10²⁰ atoms/cm²-sec. Comparison of these evaporation rates with

those given in Figure 16 shows that they are consistent with the evaporation rate of boron from pure boron at temperatures of about 2710 °K ($\sim 4 \times 10^{20}$ atoms/cm²-sec) or about 135 °K above of the melting point. Given the respective experimental uncertainties in these measurements, and previous boron vapor pressure measurements, this result can be taken as yielding evaporation rates comparable to those expected at the melting point of pure boron. This result is consistent with the intense incandescence of Probe-2 observed during each discharge as viewed on the probe TV camera, the persistence of this glow for over 4 sec after the discharge, and the obvious melted appearance of Probe-2 after exposure as evident in Figures 10(a) and 10(b). A thin film of B₄C contamination resulting from a reaction between the high temperature boron and the graphite-felt would tend to require higher ablation temperatures (~ 2900 °K) to achieve the same evaporation rate.[17] Since the boron in Probe-2 was trapped as 40 μ diameter particles within the confines of the graphite felt, and occupied 86% of the weight of the probe, a possible small B₄C contamination may not have had a significant effect on the boron evaporation rate. However, in the absence of accurate temperature measurements under controlled ablation conditions, it is difficult to resolve the respective contributions of evaporation from the pure boron particles in the graphite felt from a possible trace B₄C impurity film due to interactions with the graphite felt matrix, the effects of spallation, and possible radiation enhancement of sublimation rates.[15]

The Probe-2 deposition thicknesses can be estimated using the measured boron weight loss of 1 g. PBX-M circular plasmas have an area of 24 m². The slightly indented, elongated plasmas used during boronization had a total surface area of about 25 m² and the passive plate surface area is about 40 m². Assuming a uniform boron deposition over the 40 cm² area of the PBX-M passive plate structure would give a mass thickness of 2.5×10^{-6} g/cm². The surfaces of the aluminium passive plate structure are clad with stainless steel (304-SS). Taking the interatomic distance on the surface of the 304-SS to be comparable to that of crystalline Fe, and assuming a B-to-Fe atom coverage of 1:1, yields a boron monolayer thickness of 2×10^{15} atoms/cm², or about a total of 70 monlayers coverage from the Probe-2 deposition. This corresponds to about 2.7 monlayers/shot or 2×10^{21} atoms/shot.

Although the above spectroscopic measurements made at a point 180° from the target probe indicated significant signals from boron species, little is known about the actual toroidal distribution of the ablated boron. In order to investigate this question, 6 stainless steel samples were obtained from the interior of PBX-M, after the venting of the vessel, about 4 weeks after the boronization. The samples were located at minor

radii about 2.0 cm to 4.5 cm greater than the LCFS. Three samples ("A-Samples") were located at the toroidal location of the target probe at the inner midplane and at the top and bottom of the plasma, respectively. The other three samples ("B-Samples") were located toroidally 180° opposite the target at the same vertical positions. Auger electron scanning measurements guided by electron microscopy studies were performed on these 6 samples. In general, the results indicated the absence of boron on the exposed samples, with the exception of trace amounts found on the midplane A-Sample located directly opposite the target probe. While it is possible to attribute some of the absence of boron on the B-Samples to deposition anisotropies, similar to those encountered in the vicinity of electrodes used in boronization with PCVD [6], the absence of boron on the A-Samples, located opposite the probe is most probably due to erosion of the boron and its eventual redeposition on surfaces far from the plasma. Evidence of boron volatilized in the form of hydrides and carboranes and removed from the vessel via the pump system would be expected to accumulate in the vacuum pump oil. It was not possible to analyze the vacuum pump oil for boron content due to its contamination with tritium activity from the D-D operations of the previous experimental campaign. This analysis will be done following future PBX-M boronizations performed earlier in subsequent experimental campaigns before the generation of measurable quantities of tritium.

In the case of Probe-1, although weight loss measurements are not available, the amount of ablated boron can be estimated using the spectroscopic measurements and Probe-2 results to calibrate the emission rate. Although for Probe-1, the B III emission at 600 msec into the discharges (Figure 3) was about a factor of 3 less than for Probe-2 (Figure 11), the insertion depths and ablation edge conditions for Probe-1 and Probe-2 were similar. Integrating the total B III emission from Probe-1 and that from Probe-2 indicated that the total integrated B III signal due to Probe-1 was 0.37 of that due to Probe-2. Assuming that this boron signal ratio was proportional to the respective amounts of boron ablated from Probes-1 and Probe-2 gives 370 mg for the Probe-1 total ablation.

Using a total boron ablation of 370 mg from the above results, from an area of 5 cm², during 40 shots gives an evaporation rate of 6×10^{-3} g/cm²-sec, or 3.5×10^{20} atom/cm²-sec. This result is very close to that obtained for Probe-2. Comparing this with the evaporation rate measurements given in Figure 16 implies a temperature of evaporation from pure boron of about 2710 °K, or within experimental uncertainty of the melting point for pure boron, as was also found for Probe-2. In Probe-1, however, the

boron resided in the binder resin of the C-C composite in the form of B_4C . In Figure 16, this ablation rate from B_4C would correspond to a temperature at about 2900^0K . The slightly greater penetration depth for Probe-1 and small differences in probe heating conditions might have been sufficient to allow for this small increase in temperature. Melted boron and B_4C diffusing to the surface may have encountered violent conditions yielding effective ablation rates closer to the evaporation rates of pure boron. As in the case of Probe-2 discussed above, accurate temperature measurements under controlled ablation conditions might help to resolve the respective contributions of evaporation from the B_4C matrix, from pure boron, the effects of spallation, and possible radiation enhancement of sublimation rates.[15]

The total Probe-1 boron deposition thickness can be estimated using the above ablation result of 370 mg, and assuming as above, its uniform deposition over the passive plate surface area of 40 cm^2 . This gives a mass thickness of $9 \times 10^{-7}\text{ g/cm}^2$ or $5 \times 10^{16}\text{ atom/cm}^2$. As above, using a boron monolayer thickness of $2 \times 10^{15}\text{ atoms/cm}^2$, gives a total of about 26 monolayers coverage from the Probe-1 deposition. This corresponds to about 0.65 monolayers/shot or $5 \times 10^{20}\text{ atoms/shot}$ for 40 NBI shots. However, as noted above, little is known above the toroidal uniformity of the boron deposition.

Electrical isolation was provided for both probes to prevent possible deleterious current flows during a disruption in plasma current. There was no evidence of any effects of disruptions on either probe. In addition, although there was no obvious evidence of boron particles on the vessel floor, it is estimated that the effects of unevaporated particles from possible gross spallations would have merely accelerated the goal of providing boronization material for the plasma, and would have provided an amount of material to the vessel floor less than that derived from normal plasma-limiter erosion during operation over many months.

4. Summary and Conclusion

Solid target boronization was performed with Probe-1 consisting of a 10.7% boronized C-C composite. The probe was inserted about 2.6 cm inside the scrapeoff layer of PBX-M plasmas. The loop voltage for neutral beam heated plasmas decreased 27% and the volt-sec consumption decreased 20%. Strong peripheral spectral lines from low-Z elements decreased by factors of about 5. The central oxygen density decreased 15-20%. Total radiated power during neutral beam injection decreased by 43%. Probe-1 surface analysis indicated significant boron depletion and some

redeposition at the edge of the depleted region. The estimated boron deposition using Probe-1 was 370 mg which if uniformly deposited over the 40 m² area of the PBX-M passive plates would have given a thickness of 9×10^{-7} g/cm², or 26 monolayers during 40 discharges. This corresponds to 0.5 monolayers per shot, or 5×10^{20} atoms/shot. The estimated evaporation rate was consistent with a probe front face temperatures at, or slightly above, the boron and B₄C melting points.

Probe-2 was inserted about 2.3 cm inside the LCFS of PBX-M plasmas. High boron yields were observed on the opposite side of the vessel during ohmic heating. This is attributed to the large accessible boron mass (19.5 g), the high B/C ratio, and the low thermal conductivity of the probe material. The weight of the ablated boron was 1 g, which if uniformly deposited over the 40 m² area of the PBX-M passive plates would have given a thickness of 2.5×10^{-6} g/cm², or 70 monolayers during 26 discharges. This corresponded to 2.7 monolayers per shot, or 2×10^{21} atoms/shot. The measured evaporation rate was consistent with a probe front face temperature at, or slightly above, the boron melting point. Probe-2 boronization exhibited improved operating conditions similar to Probe-1, but for some parameters a smaller percentage change occurred due to the previous boronization using Probe-1. The Probe-2 exhibited intense melting of boron. Similar desirable percentage decreases in oxygen radiation and improvements in important operating parameters were observed in TdeV after boronization using the STB technique,[10] and after PCVD in TEXTOR [3] and ASDEX [4] using hydrogenated diborane (B₂H₆), in TFTR [5] and DIII-D [6] using deuterated diborane (D₂B₆), in JT-60U using hydrogenated decaborane (B₁₀H₁₄) [7] and in TdeV using hydrogenated trimethylborane B(CH₃)₃ [8]. In view of the different internal geometries, operating procedures, and vacuum wall conditions in these experiments, the TdeV [8,10] and PBX-M results indicate that the STB and PCVD techniques are equally effective in suppressing oxygen radiation and yielding improvements in important operating parameters. The initial applications of the STB technique using the plasma ablation of boronized probes on TdeV and PBX-M have demonstrated the effectiveness of this boronization method and avoided many of the difficulties associated with the use of hazardous borane compounds. Little is known, however, on the limitations and the possible potentials of this technique. Issues for future research interest include the merits and possible applications for probes employing different methods of introducing and maintaining the boron in various matrixes, the minimization of matrix codeposition, the detailed surface conditions at boron melting temperature under high temperature plasma edge conditions, and determining optimum deposition rates and durations between applications.

Acknowledgments

We wish to acknowledge the helpful contributions of G. Gettelfinger, J. Semler, E. Thorsland, and the PBX-M Technical Staff. The PBX-M project is supported by the U.S. Department of Energy Contract No. DE-AC02-76-CHO3073.

References

1. R. E. Bell, *et al.*, "Control of Plasma Shape and Performance of the PBX-M Tokamak Experiment in High- β_t / High- β_p Regimes", *Phys. Fluids*, **B2(6)**, 1271 (1990).
2. R. Kaita *et al.*, "Current and Pressure Profile Modification Experiments with Lower Hybrid Current Drive and Ion Bernstein Wave Heating in PBX-M", in *Proceedings of the 14th International Conference on Plasma Physics and Controlled Nuclear Fusion Research*, IAEA-CN-56/H-1-2, Wurzburg, Germany, 30 September - 7 October 1992, IAEA, Vienna.
3. J. Winter, *et al.*, "Boronization in Textor", *J. Nucl. Mater.*, **162-164**, 713 (1989).
4. U. Schneider, *et al.*, "Boronization of ASDEX", *J. Nucl. Mater.*, **176 & 177**, 350 (1990).
5. H. F. Dylla, "Effects of Boronization of the First Wall in TFTR", *J. Nucl. Mater.*, **176 & 177**, 337 (1990).
6. G. L. Jackson, *et al.*, "Boronization in DIII-D", *J. Nucl. Mater.*, **196-198**, 236 (1992).
7. M. Shimada *et al.*, "JT-60U High Power Heating Experiments", in *Proceedings of the 14th International Conference on Plasma Physics and Controlled Nuclear Fusion Research*, IAEA-CN-56/A-1-3, Wurzburg, Germany, 30 September - 7 October 1992.
8. C. Boucher, *et al.*, "Comparison of Three Boronization Techniques in TdeV", *J. Nucl. Mater.*, **196-198**, 587 (1992).
9. P.H. La Marche *et al.*, "The Diborane Gas Injection and Exhaust System for the Tokamak Fusion Test Reactor", in *Proceedings of the 16th Symposium on Fusion Technology* London 3-7 September 1990.
10. Y. Hirooka, *et al.*, "Solid Target Boronization in the Tokamak de Varennes: A Technique for Real-Time Boronization", *Nucl. Fus.* **32(11)**, 2029 (1992).

11. D. J. D. Hartog, *et al.*, "B₄C Solid Target Boronization of the MST Reversed-Field Pinch", University of Wisconsin, Report DOE/ER/53198-205, October 1992.
12. Y. Hirooka and R.W. Conn, "A Review of Materials Erosion and Redeposition Research at UCLA for the Development of Plasma-Facing Components in ITER", IPFR, University of California, Los Angeles, Report UCLA PPG #1478, March 1993, and to be published in *Atomic and Plasma-Material Interaction Processes in Controlled Fusion*, ed. R. Janev, IAEA, (1993), Vienna.
13. R. Kaita *et al.*, "Two-Dimensional Hard X-ray Imaging Diagnostic for Lower Hybrid Current Drive Experiments in PBX-M", *Rev. Sci. Instrumen.*, **61**(10), 2756 (1990).
14. R. Brakel, *et al.*, "Bulk-boronized Limiter Operation in the Wendelstein 7-AS Stellarator", *J. Nucl. Mater.*, **196-198**, 431 (1992).
15. E. Vietzke, *et al.*, "Radiation Enhanced Sublimation of Boron Containing Carbon Materials", *J. Nucl. Mater.*, **176 & 177**, 481 (1990).
16. R. A. Andrievskii, *et al.*, "Vapor Pressure and Evaporation Coefficient of Boron", *Teplofizika Vysokikh Temperatur*, **20**(5), 862 (1982). Translation in *High Temperature*, **20**(5), 697 (1982).
17. R. W. Mar and R.G. Bedford, "The Sublimation of Boron", *High Temperature Science*, **8**, 365 (1976).
18. A. W. Searcy and C. E. Myers, "The Heat of Sublimation of Boron and the Gaseous Species of the Boron-Boric Oxide System", *J. Phys. Chem.*, **61**(7), 957 (1957).
19. H. E. Robson and P.W. Gilles, "The High Temperature Vaporization Properties of Boron Carbide and the Heat of Sublimation of Boron", *J. Phys. Chem.*, **68**(5), 983 (1964).
20. D. L. Hildenbrand and W. F. Hall, "The Decomposition Pressure of Boron Carbide and the Sublimation of Boron", *J. Phys. Chem.*, **68**(5), 989 (1964).

21. Y. S. Touloukian, ed., "Thermodynamic Properties of High Temperature Solid Materials", Vol. 1: Elements, Thermophysical Properties Research Center, Purdue University, 1967.

Figure Captions

- Figure 1 (a) Photograph showing a side view of Probe-1 after exposure, and (b) photograph showing the front view of Probe-1 after exposure. The boron depleted region indicated in Figure 1(b) is visible at the center of the probe tip.
- Figure 2 The results of energy-dispersive type characteristic x-ray analysis of the surface of Probe-1 after exposure. Shown are the residual atomic percentages of boron which indicate a boron depleted region and the redeposited boron region relative to the incident ion direction.
- Figure 3 Probe-1 major radius position (cm) and the relative intensities of the B III and O II components from 600 to 620 msec (normalized to line density) versus shot number.
- Figure 4 Relative visible spectral intensities during neutral beam injection from 600 to 620 msec (normalized to line density) (a) before boronization, and (b) during boronization with Probe-1.
- Figure 5 Time evolution of relative B III and O II intensities during neutral beam injection from 400 to 700 msec (normalized to line density) (a) before, and (b) during boronization with Probe-1.
- Figure 6 Relative U.V. spectral intensities from 600 to 620 msec (normalized to line density) (a) before boronization, and (b) during boronization with Probe-1.
- Figure 7 Selected relative intensities of carbon and fluorine species from 500 to 520 msec (normalized to line density) versus shot number during boronization with Probe-1.

- Figure 8 Selected relative intensities of oxygen species from 500 to 520 msec (normalized to line density) versus shot number during boronization with Probe-1.
- Figure 9 (a) Single-turn loop voltages before and after boronization with Probe-1 for a 240 kA ohmically heated fiducial plasma discharges. The loop voltage at 600 ms decreased 20 % after boronization with Probe-1. (b) Single-turn loop voltages before and after boronization with Probe-1 for a 250 kA, 1.1 MW neutral beam heated fiducial plasma. The loop voltage at 600 ms decreased 29 % after boronization with Probe-1.
- Figure 10 (a) Photograph showing a top side view of Probe-2 held in its C-C composite holder after exposure to PBX-M plasmas. Shown is the resolidified boron melted during the ablation process. The incident ion direction is from the left. The separation between the two halves of the probe material is due to the effect of the melting boron (refer to text). (b) Photograph of Probe-2 after exposure showing the side facing the incident ions. The boron appears to have undergone more intense melting on the side facing the incident ions.
- Figure 11 Probe-2 major radius position (cm) and the relative intensities of the B III and O II components from 600 to 620 msec (normalized to line density) versus shot number.
- Figure 12 Relative visible spectral intensities during ohmic plasmas from 600 to 620 msec (normalized to line density) (a) before boronization, and (b) during boronization with Probe-2.
- Figure 13 Time evolution of relative B III and O II intensities during ohmic plasmas (normalized to line density) (a) before, and (b) during boronization with Probe-2.
- Figure 14 Relative U.V. spectral intensities from 600 to 620 msec (normalized to line density) (a) before boronization, and (b) during boronization with Probe-2.

Figure 15 Total D-D neutron production rates (n/sec) versus neutral beam injected power for discharges heated with 300 msec of deuterium neutral beam injection before boronization, during Probe-1 boronization, and after Probe-1 plus Probe-2 boronization.

Figure 16 Boron evaporation rates (Atoms/cm²-sec) versus temperature derived from vapor pressure measurements using the Knudsen equation. The indicated measurements are as follows; (a) Ref. 16, W electrodes, uncorrected for impurity film, (b) Ref. 16, W electrodes, corrected for impurity film, (c) Ref. 17, ZrB₂ crucible, (d) Ref.18, C crucible, (e) Ref. 18, Ta crucible, (f) Ref. 18, ZrB₂ crucible, (g) Ref. 19, graphite crucible, (h) Ref. 20, graphite crucible. The relatively large variations in the earlier results for pure boron are due in part to impurity effects resulting from boron-graphite crucible interactions which were reduced in later measurements.

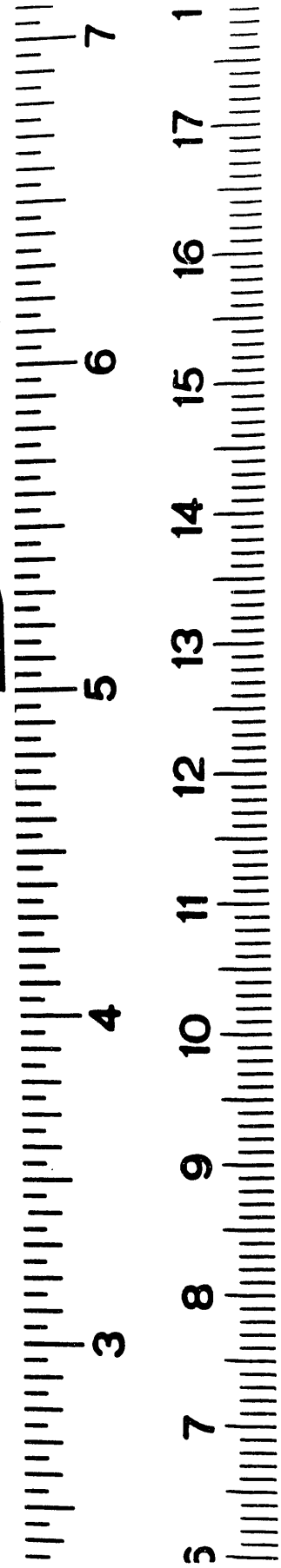
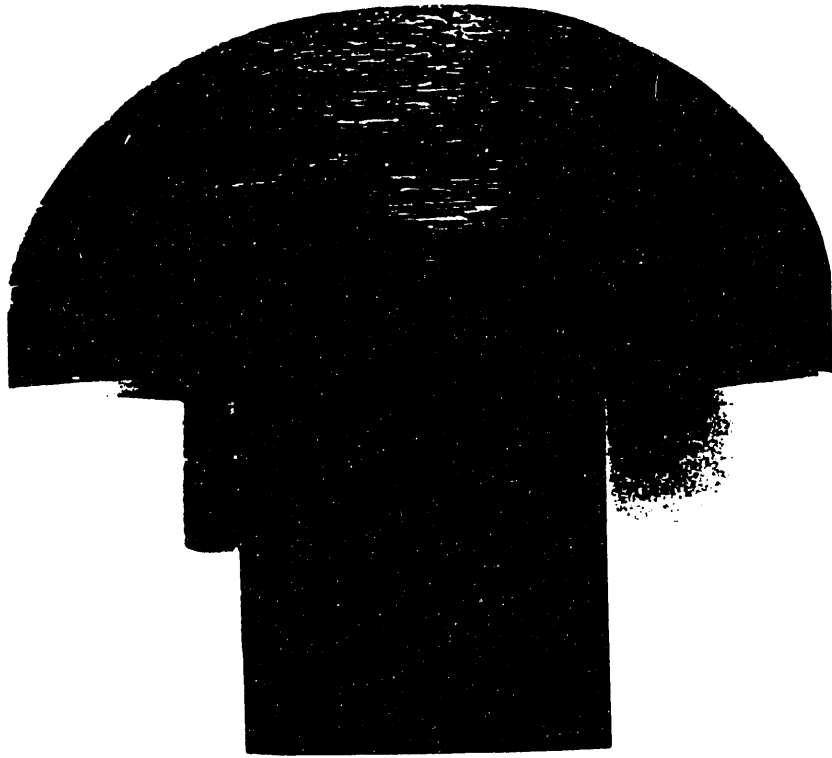
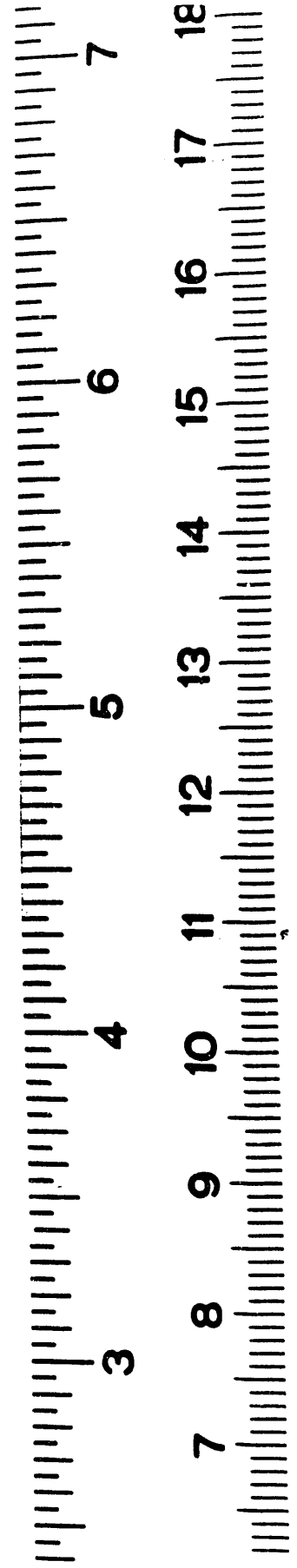
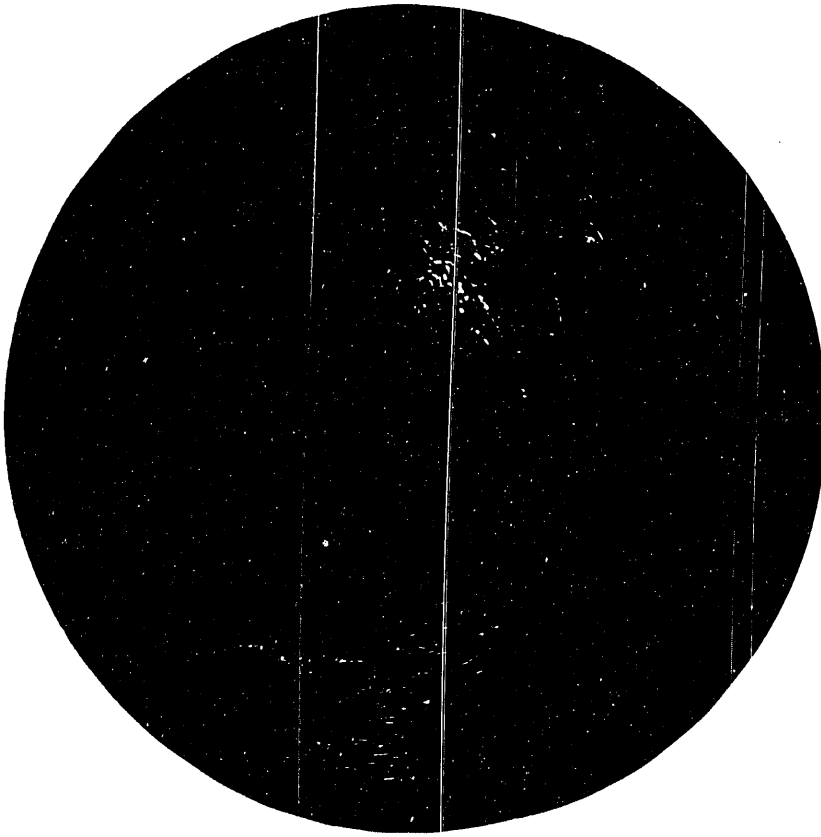
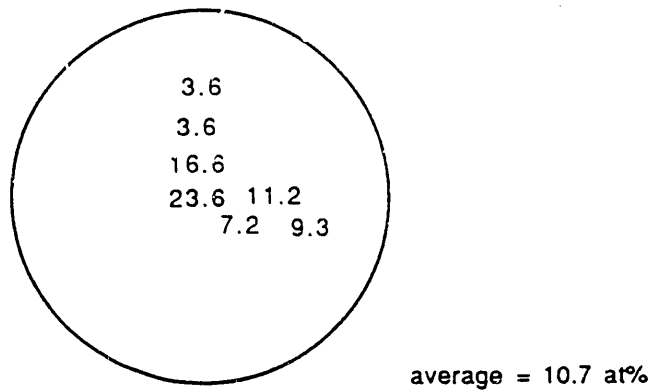


Fig. 1(a)

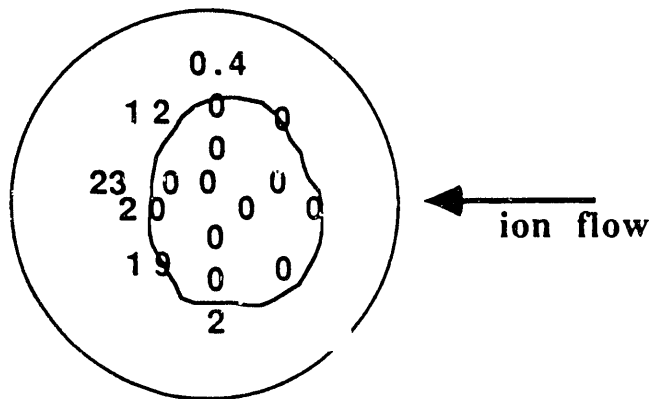


Boron analysis by EDX

As recieved



Boron at% map after exposure
in PBX



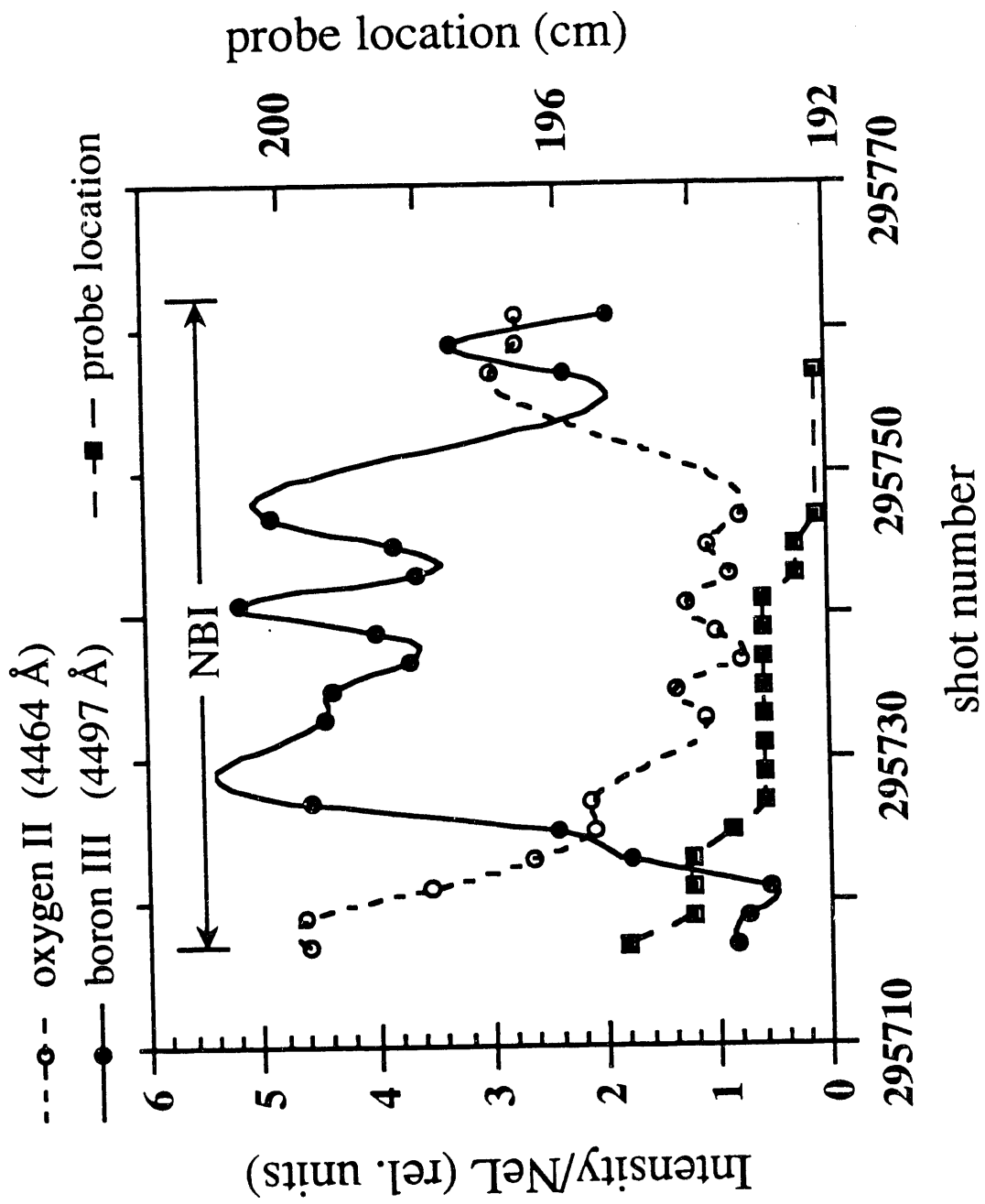
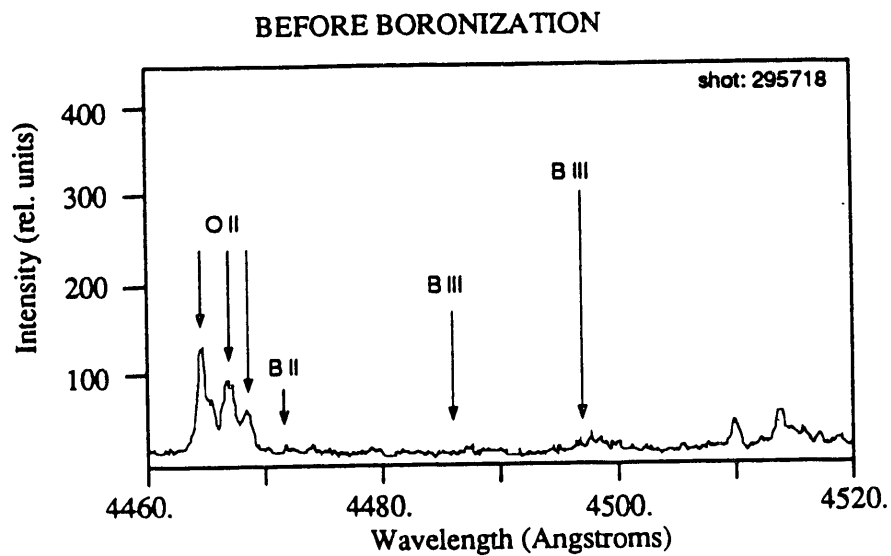
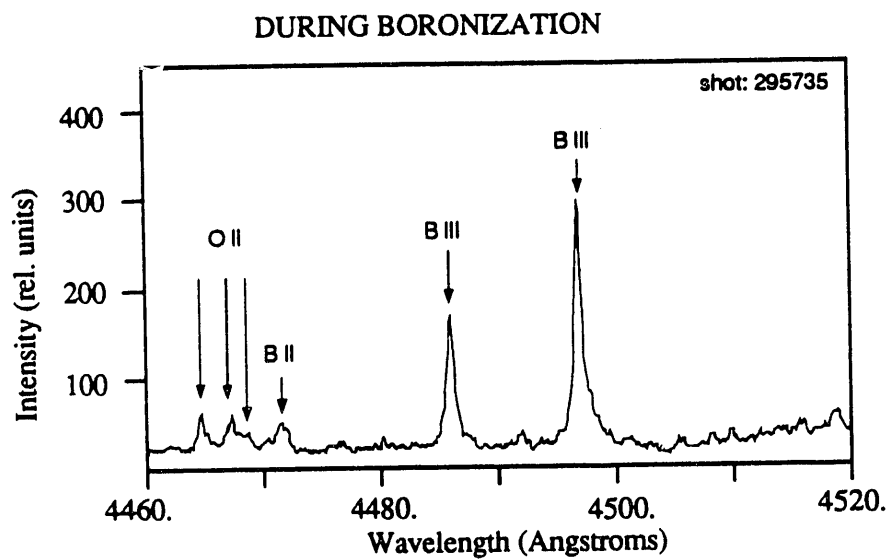


Fig 3

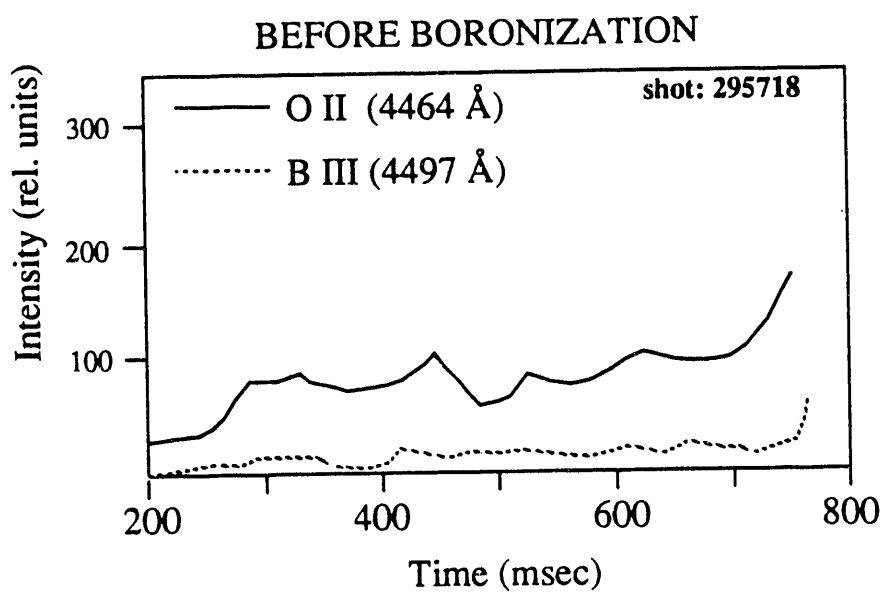
a)



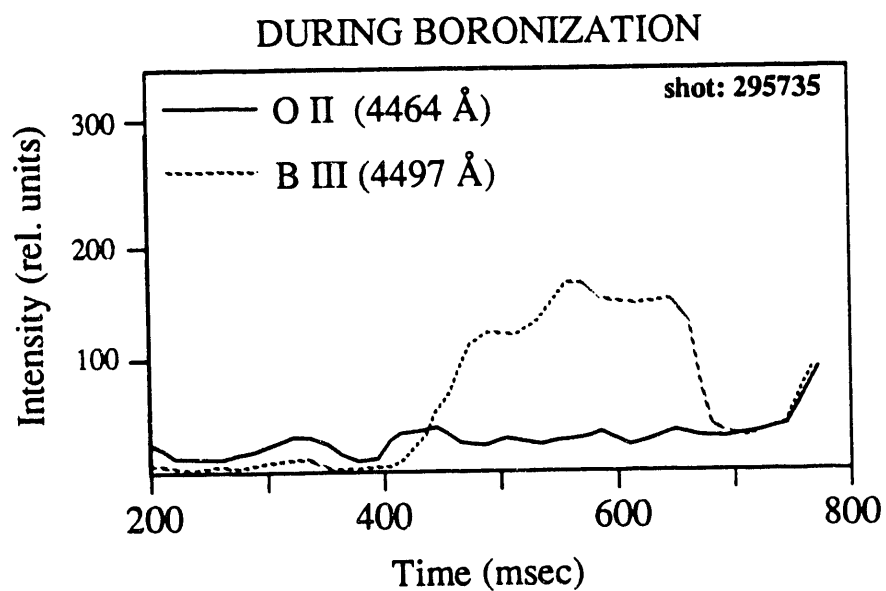
b)



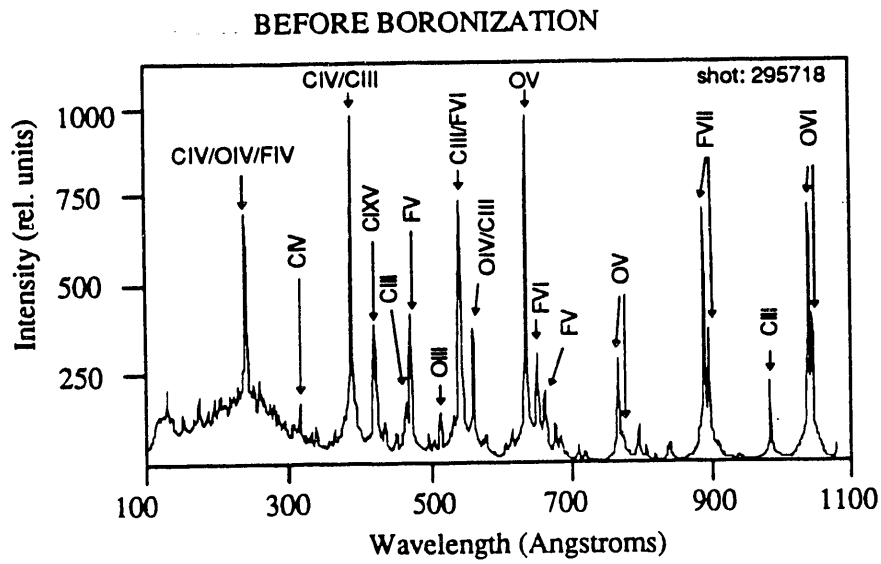
a)



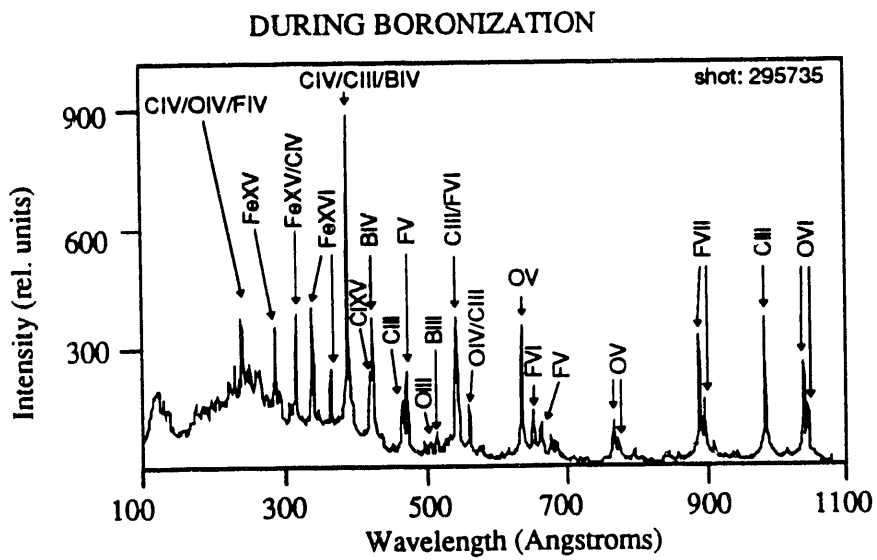
b)



a)



b)



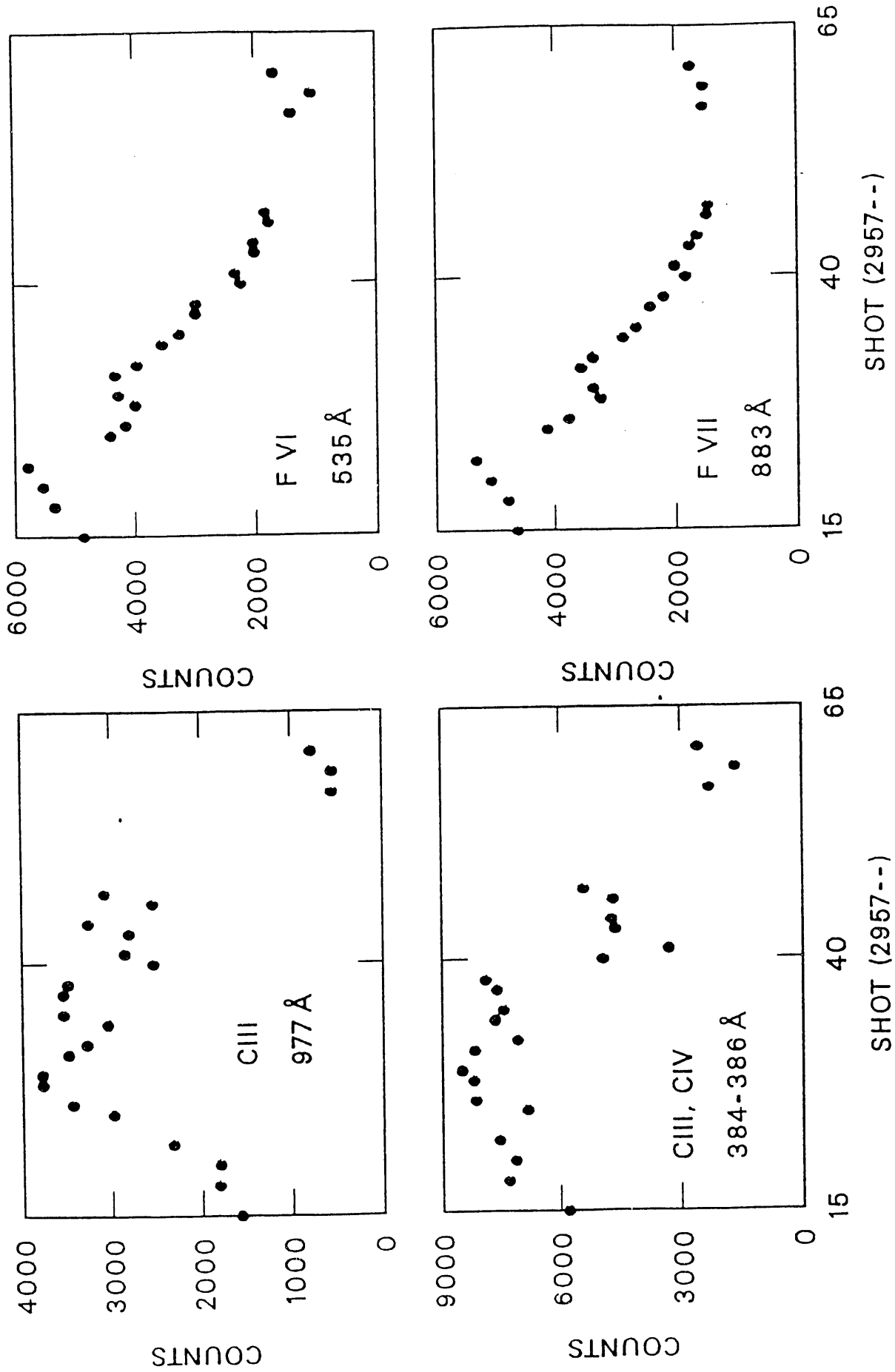


Fig. 7

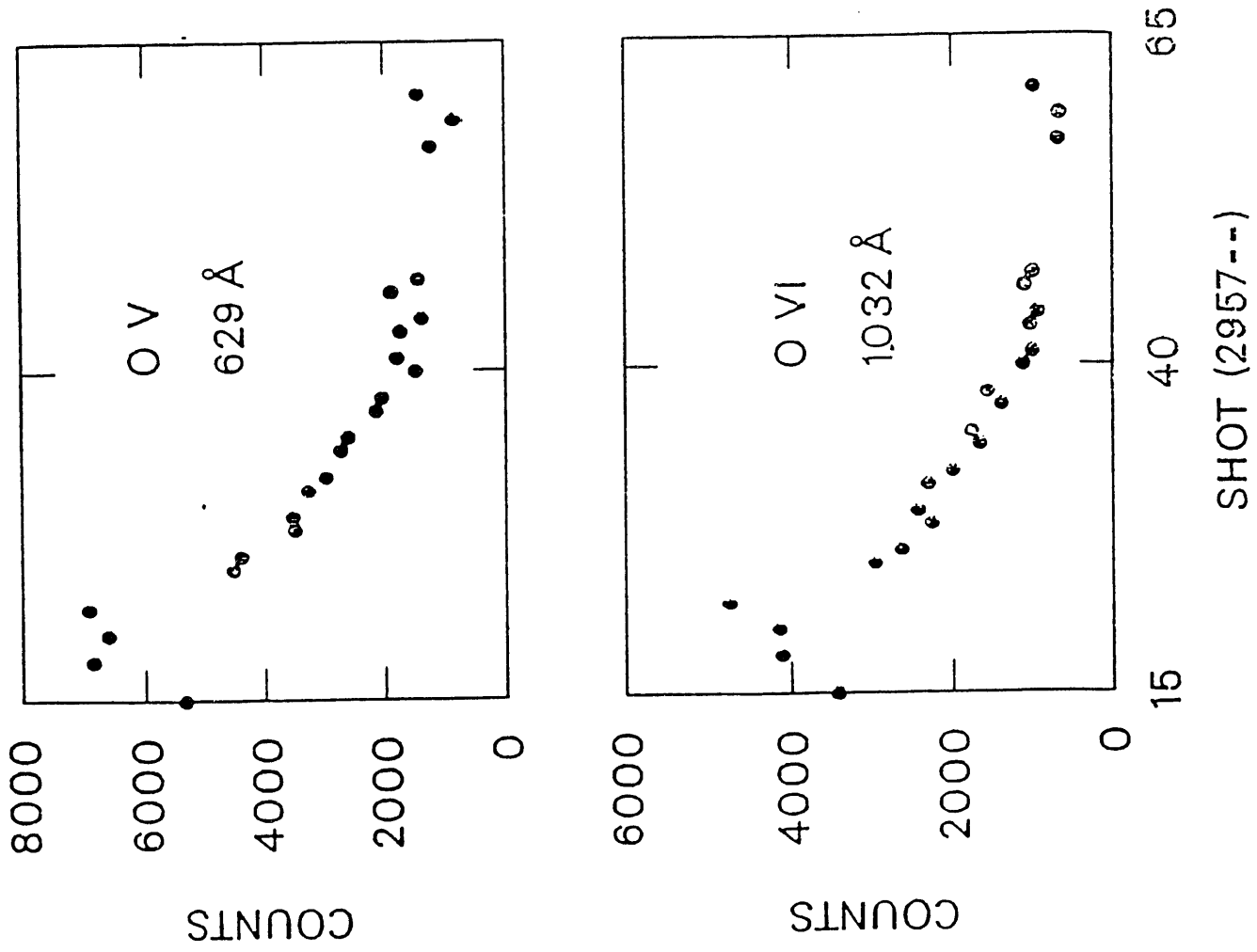
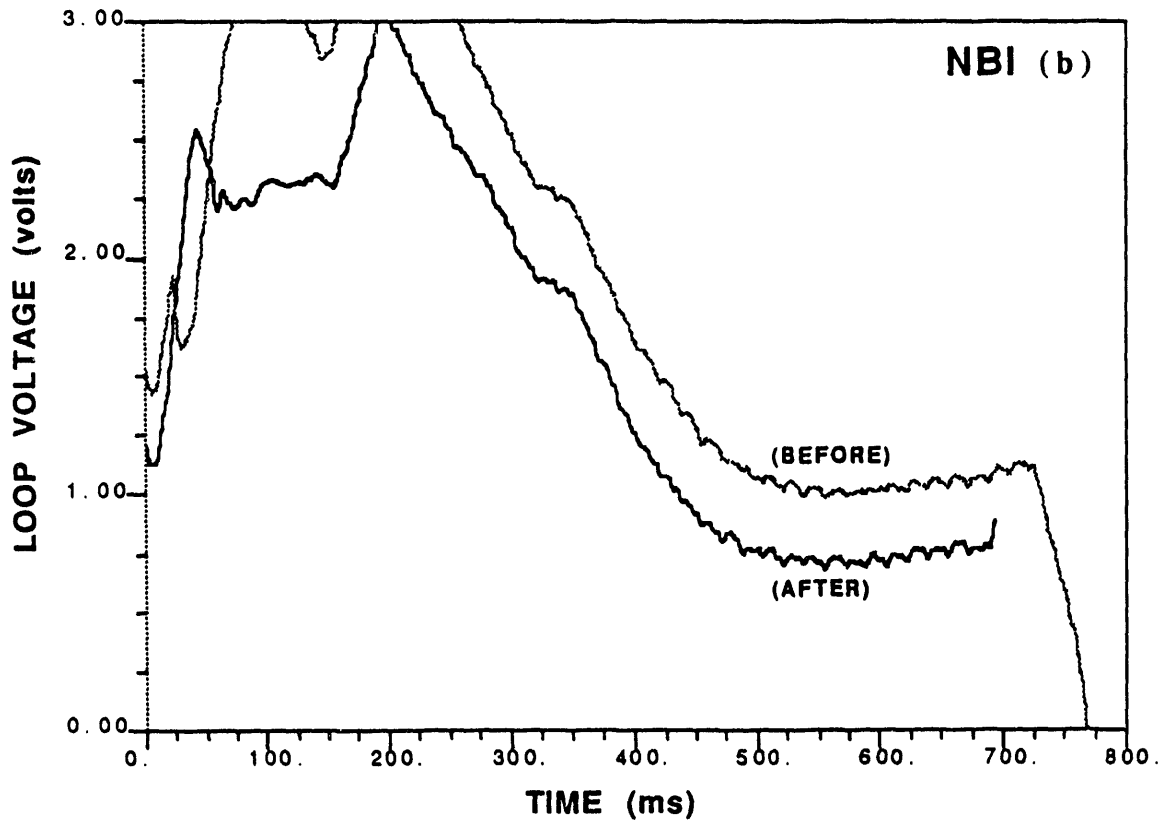
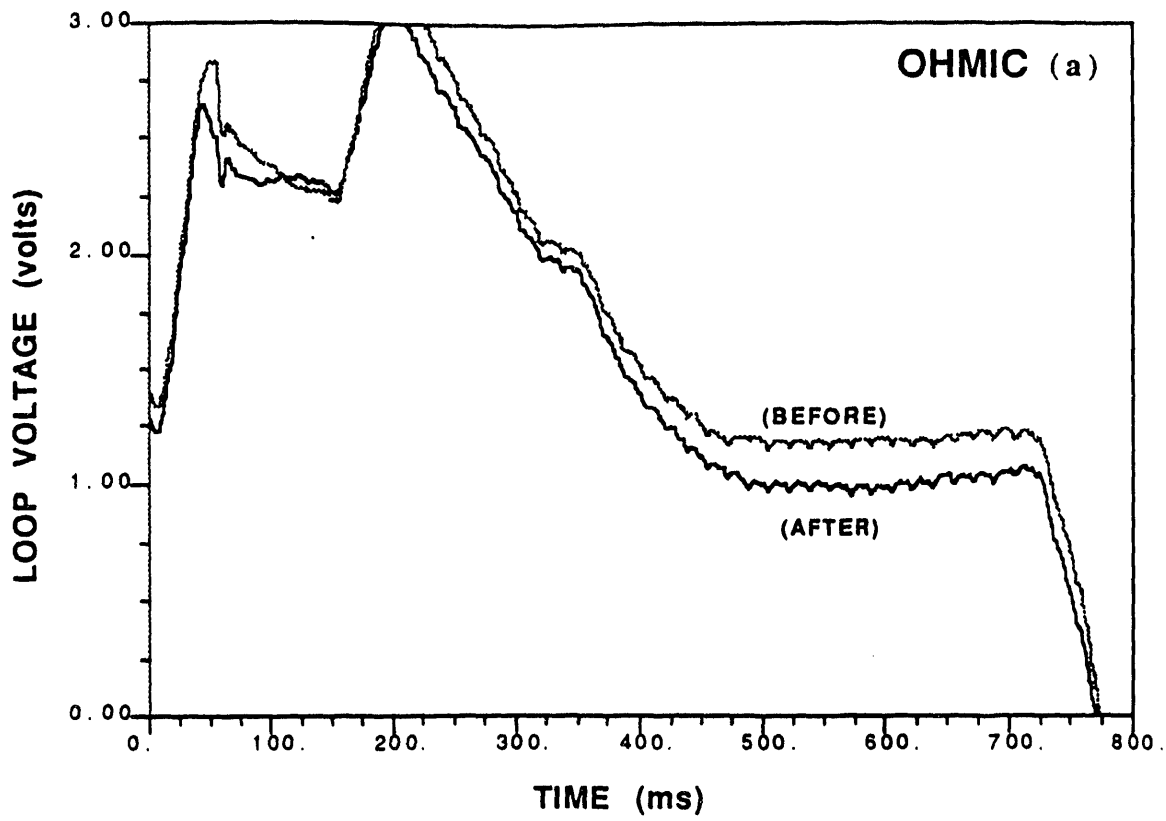
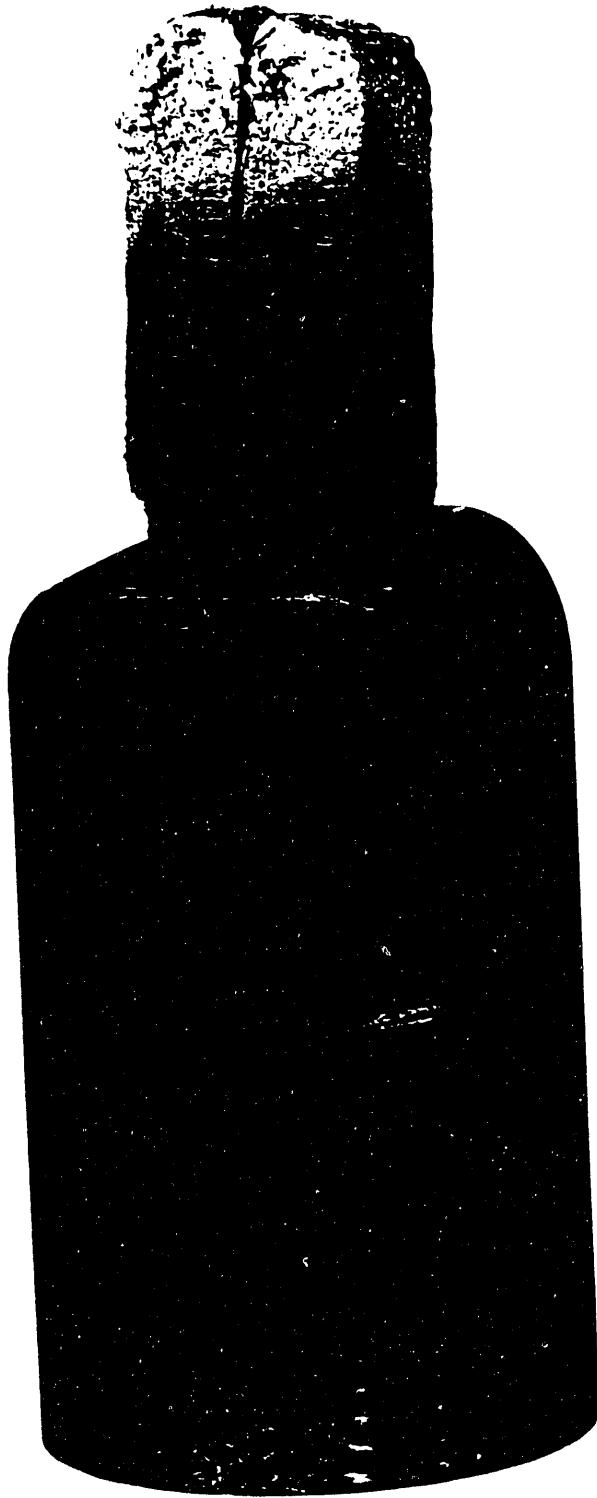
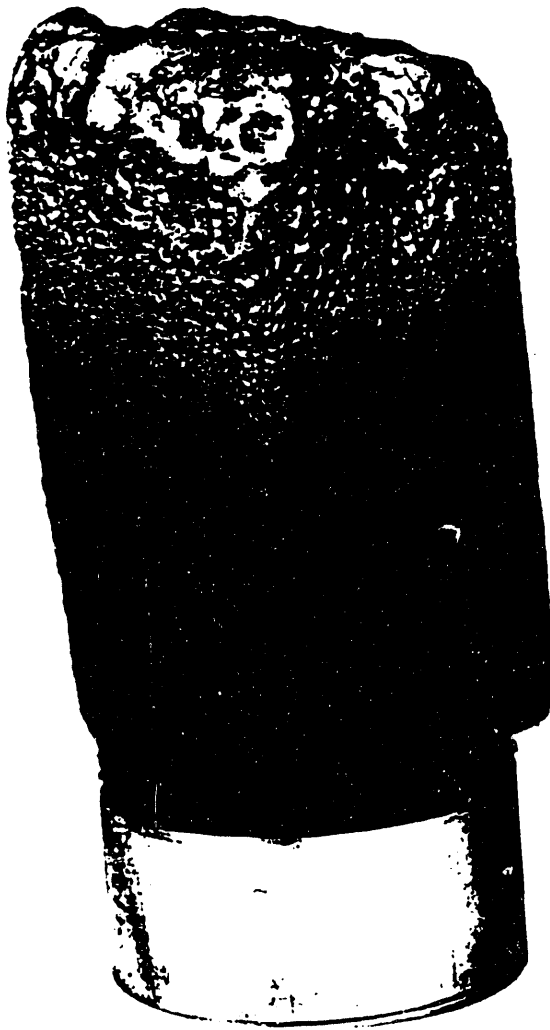


Fig. 2







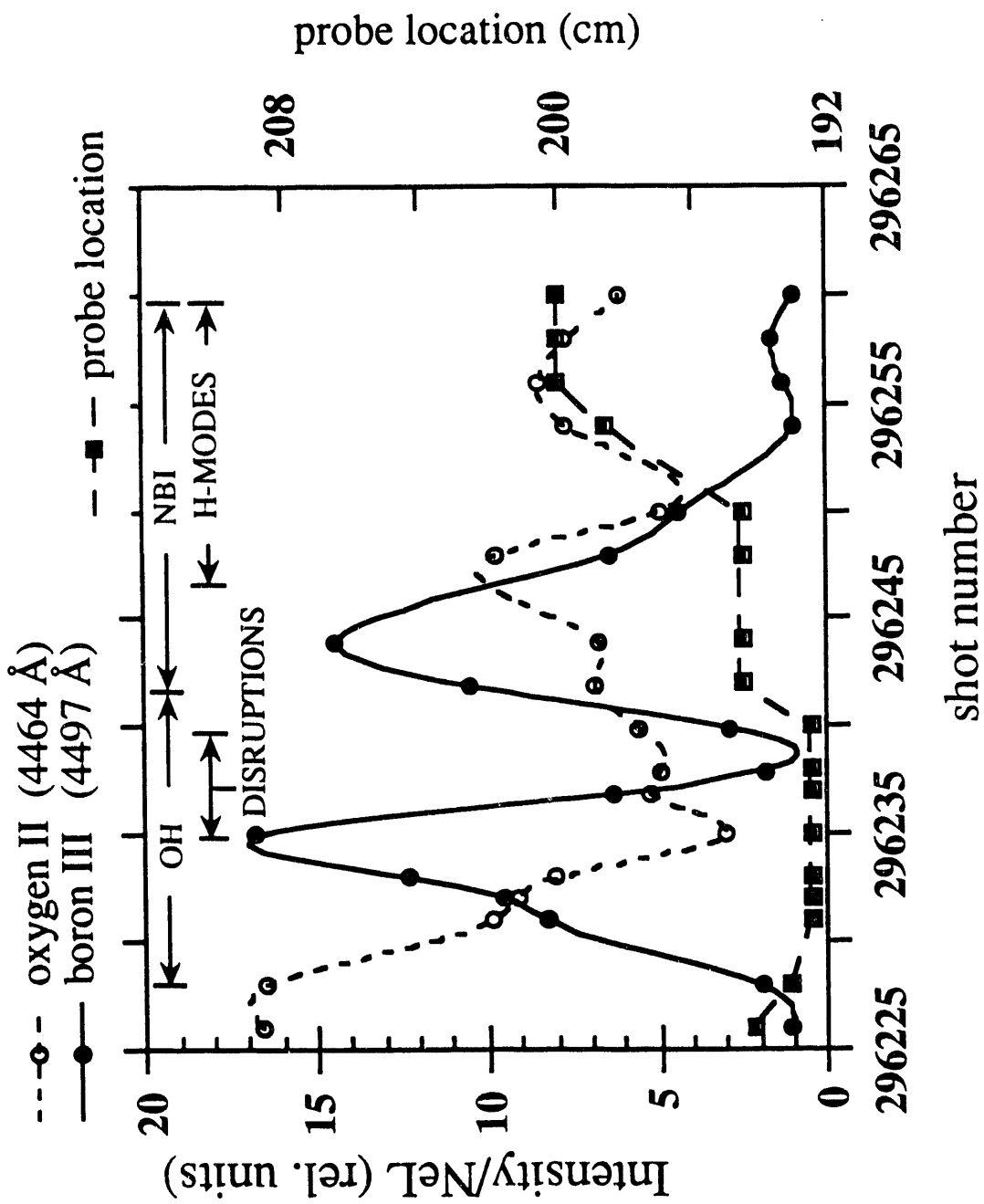
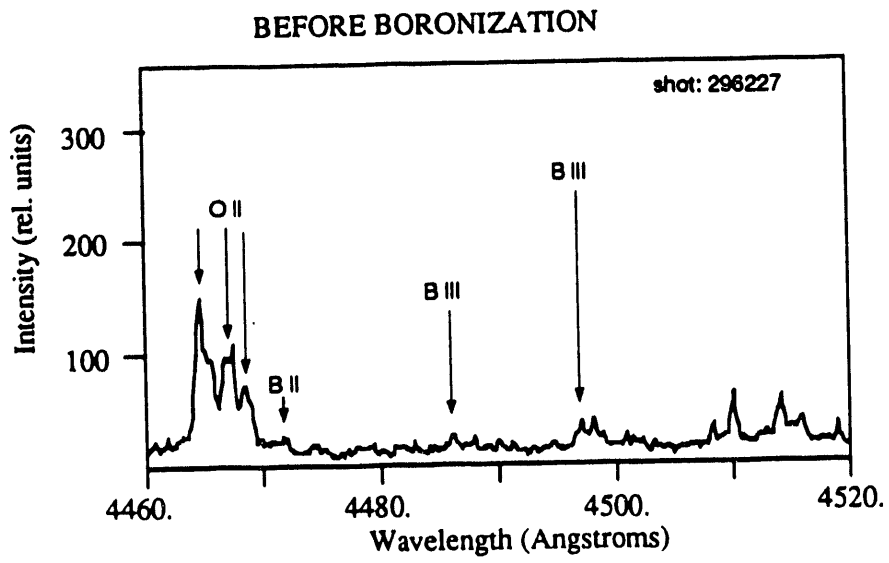
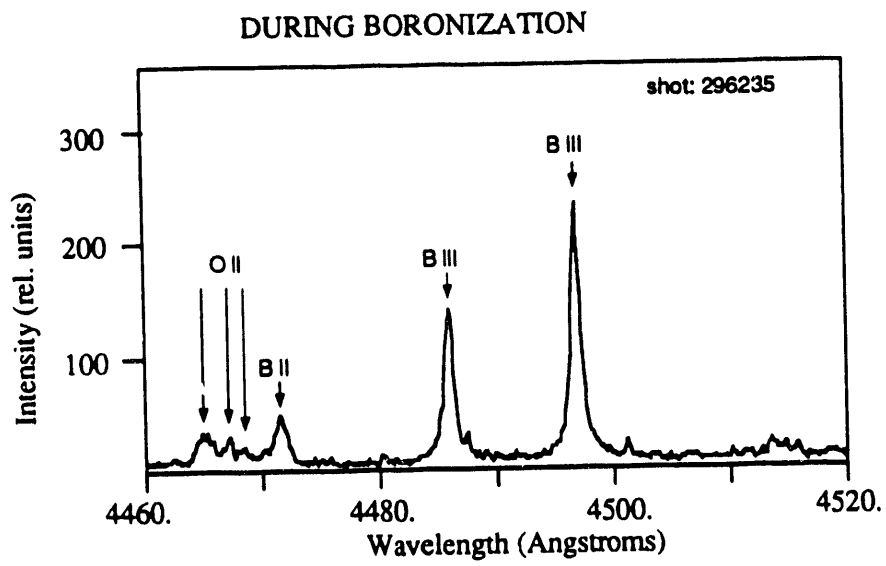


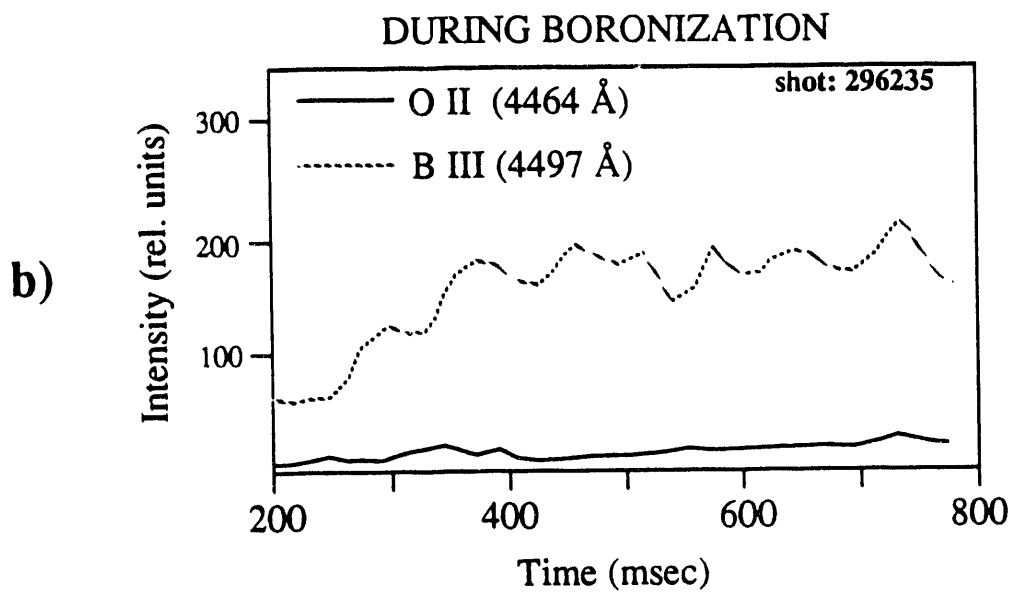
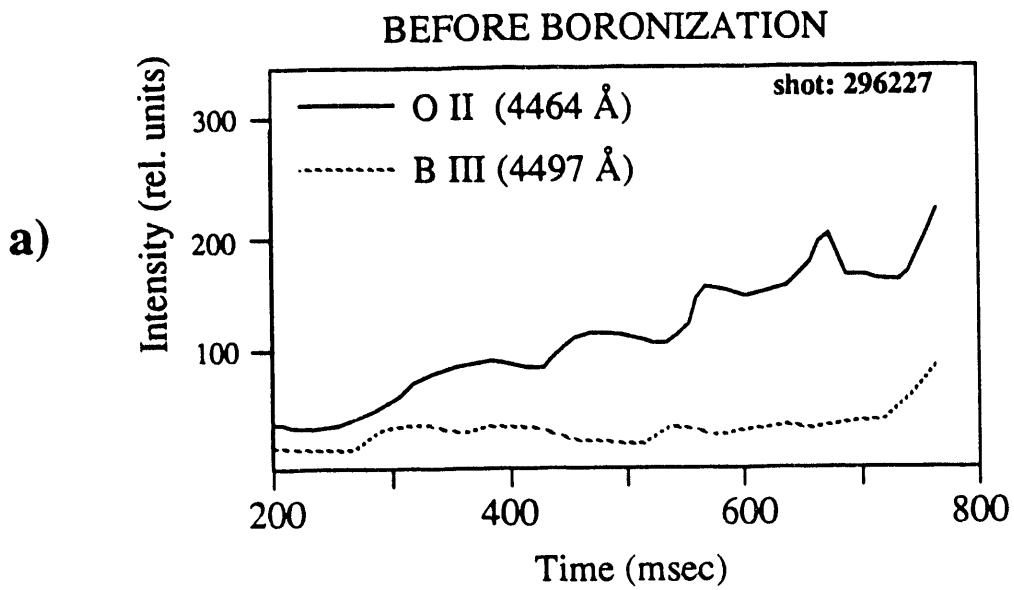
Fig. 11

a)

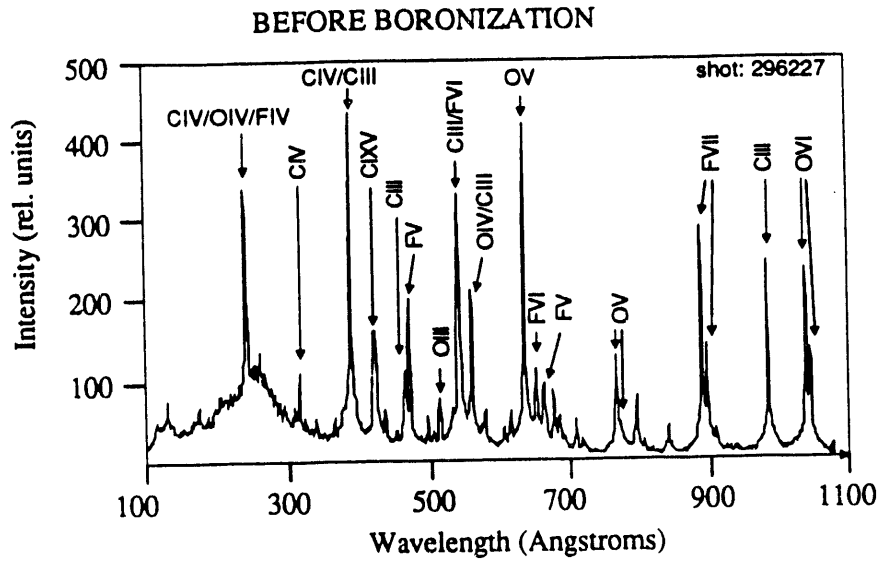


b)

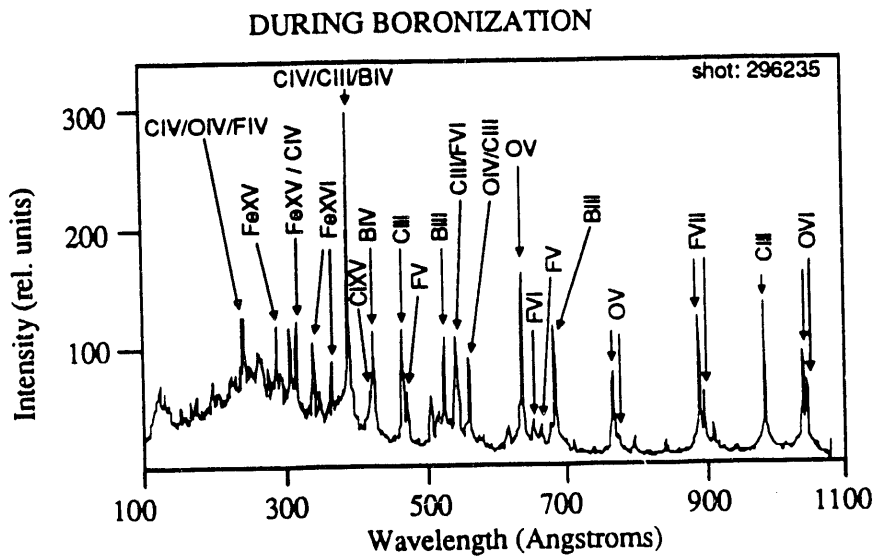


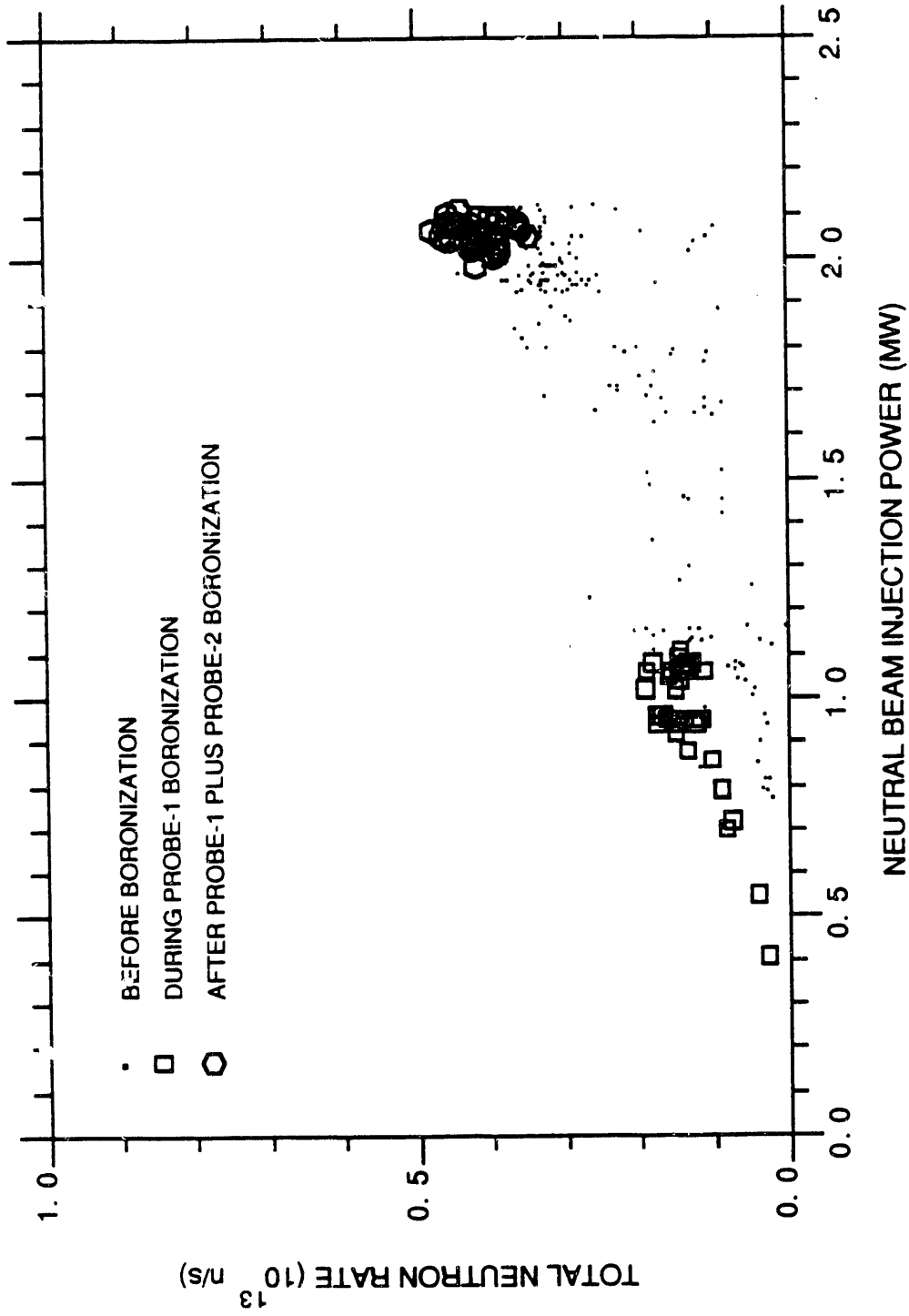


a)



b)





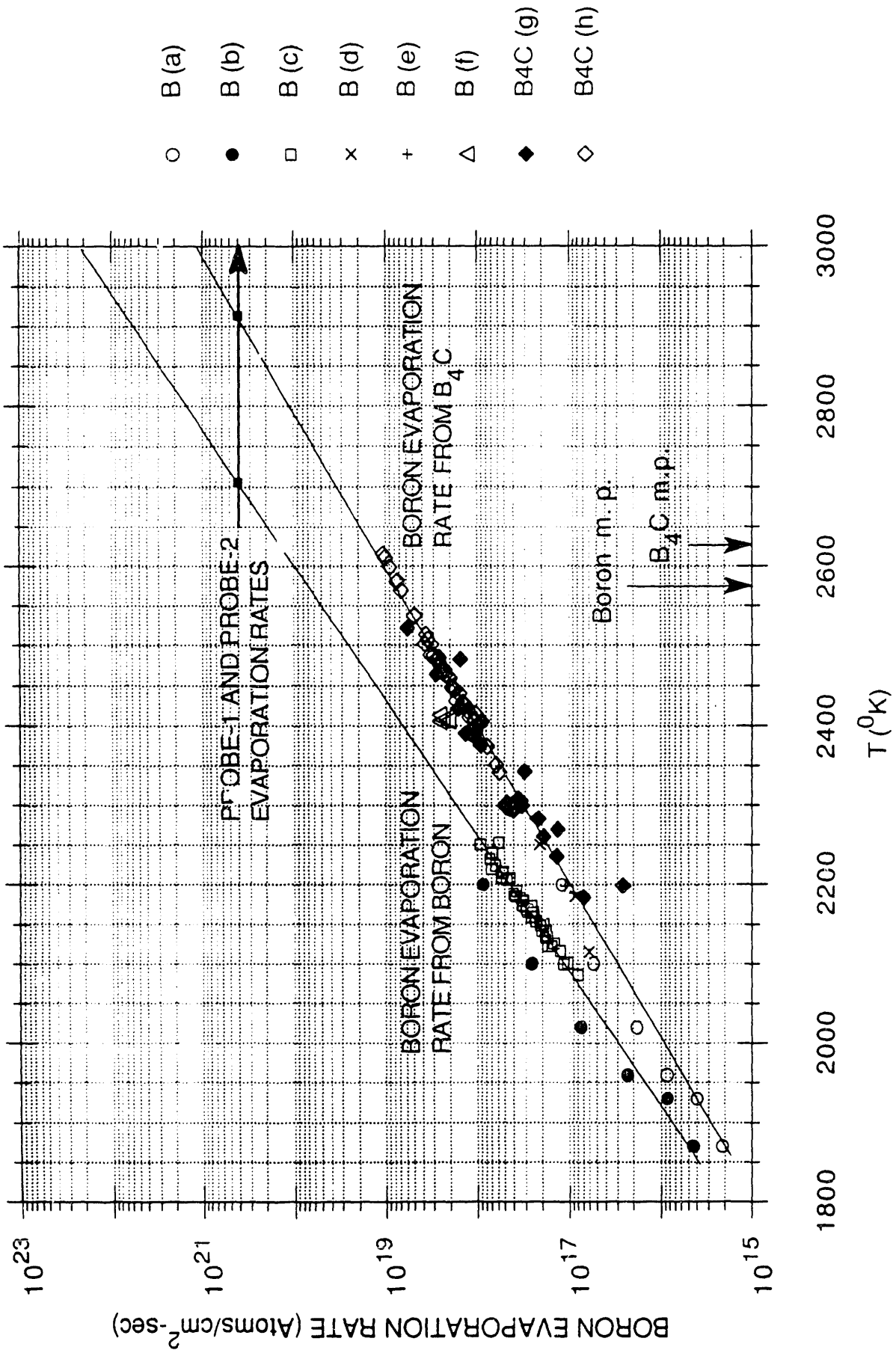


Fig. 16

EXTERNAL DISTRIBUTION IN ADDITION TO UC-420

Dr. F. Paoloni, Univ. of Wollongong, AUSTRALIA
 Prof. M.H. Brennan, Univ. of Sydney, AUSTRALIA
 Plasma Research Lab., Australian Nat. Univ., AUSTRALIA
 Prof. I.R. Jones, Flinders Univ, AUSTRALIA
 Prof. F. Cap, Inst. for Theoretical Physics, AUSTRIA
 Prof. M. Heindler, Institut für Theoretische Physik, AUSTRIA
 Prof. M. Goossens, Astronomisch Instituut, BELGIUM
 Ecole Royale Militaire, Lab. de Phy. Plasmas, BELGIUM
 Commission-European, DG. XII-Fusion Prog., BELGIUM
 Prof. R. Boucqué, Rijksuniversiteit Gent, BELGIUM
 Dr. P.H. Sakemaka, Instituto Fisica, BRAZIL
 Instituto Nacional De Pesquisas Espaciais-INPE, BRAZIL
 Documents Office, Atomic Energy of Canada Ltd., CANADA
 Dr. M.P. Bachynski, MPB Technologies, Inc., CANADA
 Dr. H.M. Skarsgard, Univ. of Saskatchewan, CANADA
 Prof. J. Teichmann, Univ. of Montreal, CANADA
 Prof. S.R. Sreenivasan, Univ. of Calgary, CANADA
 Prof. T.W. Johnston, INRS-Energie, CANADA
 Dr. R. Bolton, Centre canadien de fusion magnétique, CANADA
 Dr. C.R. James., Univ. of Alberta, CANADA
 Dr. P. Lukác, Komenského Univerzita, CZECHO-SLOVAKIA
 The Librarian, Culham Laboratory, ENGLAND
 Library, R61, Rutherford Appleton Laboratory, ENGLAND
 Mrs. S.A. Hutchinson, JET Library, ENGLAND
 Dr. S.C. Sharma, Univ. of South Pacific, FIJI ISLANDS
 P. Mähönen, Univ. of Helsinki, FINLAND
 Prof. M.N. Bussac, Ecole Polytechnique., FRANCE
 C. Mouttet, Lab. de Physique des Milieux Ionisés, FRANCE
 J. Radet, CEN/CADARACHE - Bat 506, FRANCE
 Prof. E. Economou, Univ. of Crete, GREECE
 Ms. C. Rinni, Univ. of Ioannina, GREECE
 Dr. T. Mui, Academy Bibliographic Ser., HONG KONG
 Preprint Library, Hungarian Academy of Sci., HUNGARY
 Dr. B. DasGupta, Saha Inst. of Nuclear Physics, INDIA
 Dr. P. Kaw, Inst. for Plasma Research, INDIA
 Dr. P. Rosenau, Israel Inst. of Technology, ISRAEL
 Librarian, International Center for Theo Physics, ITALY
 Miss C. De Palo, Associazione EURATOM-ENEA, ITALY
 Dr. G. Grosso, Istituto di Fisica del Plasma, ITALY
 Prof. G. Rostangni, Istituto Gas Ionizzati Del Cnr, ITALY
 Dr. H. Yamato, Toshiba Res & Devel Center, JAPAN
 Prof. I. Kawakami, Hiroshima Univ., JAPAN
 Prof. K. Nishikawa, Hiroshima Univ., JAPAN
 Director, Japan Atomic Energy Research Inst., JAPAN
 Prof. S. Itoh, Kyushu Univ., JAPAN
 Research Info. Ctr., National Instit. for Fusion Science, JAPAN
 Prof. S. Tanaka, Kyoto Univ., JAPAN
 Library, Kyoto Univ., JAPAN
 Prof. N. Inoue, Univ. of Tokyo, JAPAN
 Secretary, Plasma Section, Electrotechnical Lab., JAPAN
 S. Mori, Technical Advisor, JAERI, JAPAN
 Dr. C. Mitarai, Kumamoto Inst. of Technology, JAPAN
 J. I yeon-Sook, Korea Atomic Energy Research Inst., KOREA
 D.I. Choi, The Korea Adv. Inst. of Sci. & Tech., KOREA
 Prof. B.S. Liley, Univ. of Waikato, NEW ZEALAND
 Inst of Physics, Chinese Acad Sci PEOPLE'S REP. OF CHINA
 Library, Inst. of Plasma Physics, PEOPLE'S REP. OF CHINA
 Tsinghua Univ. Library, PEOPLE'S REPUBLIC OF CHINA
 Z. Li, S.W. Inst Physics, PEOPLE'S REPUBLIC OF CHINA
 Prof. J.A.C. Cabral, Instituto Superior Tecnico, PORTUGAL
 Dr. O. Petrus, AL I CUZA Univ., ROMANIA
 Dr. J. de Villiers, Fusion Studies, AEC, S. AFRICA
 Prof. M.A. Hellberg, Univ. of Natal, S. AFRICA
 Prof. D.E. Kim, Pohang Inst. of Sci. & Tech., SO. KOREA
 Prof. C.I.E.M.A.T, Fusion Division Library, SPAIN
 Dr. L. Stanflo, Univ. of UMEA, SWEDEN
 Library, Royal Inst. of Technology, SWEDEN
 Prof. H. Wilhelmson, Chalmers Univ. of Tech., SWEDEN
 Centre Phys. Des Plasmas, Ecole Polytech, SWITZERLAND
 Bibliothek, Inst. Voor Plasma-Fysica, THE NETHERLANDS
 Asst. Prof. Dr. S. Cakir, Middle East Tech. Univ., TURKEY
 Dr. V.A. Glukhikh, Sci. Res. Inst. Electrophys. Apparatus, USSR
 Dr. D.D. Ryutov, Siberian Branch of Academy of Sci., USSR
 Dr. G.A. Eliseev, I.V. Kurchatov Inst., USSR
 Librarian, The Ukr.SSR Academy of Sciences, USSR
 Dr. L.M. Kovrizhnykh, Inst. of General Physics, USSR
 Kernforschungsanlage GmbH, Zentralbibliothek, W. GERMANY
 Bibliothek, Inst. Für Plasmaforschung, W. GERMANY
 Prof. K. Schindler, Ruhr-Universität Bochum, W. GERMANY
 Dr. F. Wegner, (ASDEX), Max-Planck-Institut, W. GERMANY
 Librarian, Max-Planck-Institut, W. GERMANY
 Prof. R.K. Janev, Inst. of Physics, YUGOSLAVIA

**DATE
FILMED**

8 / 23 / 93

END

